

HYPERBOLICITY-PRESERVING AND WELL-BALANCED STOCHASTIC GALERKIN METHOD FOR SHALLOW WATER EQUATIONS*

DIHAN DAI[†], YEKATERINA EPSHTEYN[†], AND AKIL NARAYAN^{†‡}

Abstract. A stochastic Galerkin formulation for a stochastic system of balanced or conservation laws may fail to preserve hyperbolicity of the original system. In this work, we develop a hyperbolicity-preserving stochastic Galerkin formulation for the one-dimensional shallow water equations by carefully selecting the polynomial chaos expansion of the nonlinear q^2/h term in terms of the polynomial chaos expansions of the conserved variables. In addition, in an arbitrary finite stochastic dimension, we establish a sufficient condition to guarantee hyperbolicity of the stochastic Galerkin system through a finite number of conditions at stochastic quadrature points. Further, we develop a well-balanced central-upwind scheme for the stochastic shallow water model and derive the associated hyperbolicity-preserving CFL-type condition. The performance of the developed method is illustrated on a number of challenging numerical tests.

Key words. finite volume method, stochastic Galerkin method, shallow water equations, hyperbolic systems of conservation law and balance laws

17 AMS subject classifications. 35L65, 35Q35, 35R60, 65M60, 65M70

18 **1. Introduction.** The classical one-dimensional deterministic Saint-Venant sys-
19 tem of shallow water equations is,

$$20 \quad (1.1) \quad \begin{aligned} (h)_t + (q)_x &= 0, \\ (q)_t + \left(\frac{q^2}{h} + \frac{1}{2}gh^2 \right)_x &= -ghB_x, \end{aligned}$$

21 where $h = h(x, t)$ is the water height, $q = q(x, t)$ is the water discharge, g is the
 22 gravitational constant, and $B = B(x)$ is the time-independent bottom topography.
 23 This system was first derived in [9] and since then has been widely used in modeling
 24 the flows whose horizontal scales are significantly larger than vertical scales, such as
 25 water flows in rivers, lakes and coastal areas. However, the accuracy and prediction
 26 capabilities of shallow water models depend strongly on the presence of various un-
 27 certainties that naturally arise in measuring or empirically approximating, e.g., the
 28 bottom topography data, or initial and boundary conditions. Hence, it is important
 29 to consider a stochastic version of the shallow water equations (SWE). In this work
 30 we focus on uncertainty that results in *parameterized* SWE, where parameters are
 31 modeled as random variables. In particular, we study the polynomial chaos ex-
 32 pansion (PCE) strategy, which is very effective when quantities of interest vary smoothly
 33 with respect to the parameters.

34 There are two widely used classes of methods for addressing uncertainty in (pa-
 35 rameterized) partial differential equations using PCE. One class, of *non-intrusive*
 36 type methods, computes stochastic quantities by generating an ensemble of solutions
 37 of realizations, each of which may be treated as a deterministic problem. Statistical
 38 information is obtained from this ensemble by post-processing the ensemble solutions.

*submitted to the editors December 24, 2020.

Funding: A. Narayan was partially supported by NSF DMS-1848508.

[†]Department of Mathematics, University of Utah, Salt Lake City, UT 84112 (dai@math.utah.edu, epshteyn@math.utah.edu).

[†]Scientific Computing and Imaging (SCI) Institute, University of Utah, Salt Lake City, UT 84112 (akil@sci.utah.edu).

39 Examples of such methods include Monte-Carlo-type methods that use randomly se-
40 lected samples, and the stochastic collocation methods that use *a priori* pre-selected
41 samples (e.g., [42, 31, 29]). Since they rely on multiple queries of existing determin-
42 istic solvers, non-intrusive methods are easy to implement and highly parallelizable,
43 but can result in less accurate approximations than the intrusive type methods.

44 The other group of methods are *intrusive* methods. Such methods typically re-
45 quire a substantial rewrite of legacy code and solvers. In the context of PCE methods,
46 the prototypical intrusive strategy is the stochastic Galerkin (SG) approach, wherein
47 one replaces an underlying stochastic process with its truncated PCE [40, 43], and then
48 forms a system of differential equations via Galerkin projection in stochastic space.
49 As a consequence, one derives a new system of partial differential equations whose
50 unknowns are (time- and space-varying) coefficients of the PCE. Intrusive methods
51 are projection-based approximations, and thus their accuracy is near-optimal in an
52 L^2 sense for static problems. Discussion on the existing convergence theory for SG
53 methods can be found, for example in [2, 27]. SG methods have been successfully em-
54 ployed for modeling uncertainty in diffusion models [44, 12], kinetic equations [17, 37],
55 and conservation and balanced laws with symmetric Jacobian matrices [39].

56 For hyperbolic systems, such as the SWE, the associated SG system may not
57 be hyperbolic in general [11, 18]. Thus, the intrusive SG formulation can result in
58 a system of differential equations of a different class than the original deterministic
59 system. There are currently several efforts to resolve this issue for more general types
60 of equations and to preserve hyperbolicity of the SG system. For quasilinear hyper-
61 bolic systems, hyperbolicity can be ensured by multiplying the SG formulation of the
62 system by the left eigenvector matrix of its flux Jacobian matrix [41]. Unfortunately
63 this transformation results in a non-conservative form and numerical solvers designed
64 for conservative formulations cannot be applied directly. A recent operator-splitting
65 based approach has been developed for both the Euler equations [8] and the SWE [7],
66 where the original systems are split into hyperbolic subsystems whose SG formulations
67 remain hyperbolic. However, this may still lead to complex eigenvalues due to the
68 mismatch in hyperbolicity sets of the subsystems [36]. Another strategy to resolve the
69 hyperbolicity issue of SG formulation is to introduce an appropriate change of vari-
70 ables. For example, the SG system of balanced/conservation laws in terms of entropic
71 variables can be shown to be hyperbolic [35, 34]. In addition, an optimization-based
72 method, called the intrusive polynomial moment method (IPMM), was proposed to
73 calculate the PCE of entropic variables given the PCE of the conserved variables
74 [11, 35, 34]. However, the optimization problem in IPMM that must be solved for
75 each cell and at each time step can be computationally expensive. There are also
76 strategies that employ Roe variable formulations: In [33, 15, 14], the flux of the SG
77 system is constructed using Roe variables and the conservative form of the system is
78 preserved. It has been shown that both the SG formulations of the Euler equation [33]
79 and the SWE [15] in terms of Roe variables are hyperbolic when using a Wiener-Haar
80 expansion. The SG formulation of the isothermal Euler equations in terms of Roe
81 variables is hyperbolic for any basis function under a positive definiteness condition
82 [15]. However, it can still be expensive to implement the Roe formulation since the
83 PCE of Roe variables need to be calculated by solving both a nonlinear equation and
84 a linear equation.

85 The SG formulation of the SWE may not be hyperbolic due to the PCE of the
86 nonlinear, non-polynomial term q^2/h [11]. This issue can be partially resolved by
87 using the Roe variables and the Wiener-Haar expansion [15, 14]. In this work, we
88 develop hyperbolicity-preserving SG PCE formulation for the SWE by carefully se-

89 lecting the PCE of q^2/h term using only the PCE of the conserved variables. Further,
 90 we establish a connection between the hyperbolicity of the SG system and the original
 91 system. Namely, we show that preserving positivity of the water height a finite num-
 92 ber of stochastic quadrature points is sufficient to preserving hyperbolicity of the SG
 93 formulation of the SWE. In addition, we will present the well-balanced discretization
 94 for our SG formulation of SWE, which preserves positivity of the water height at
 95 certain quadrature points in the stochastic domain. In this paper, we adopt the filter
 96 from [36] to ensure the positivity-preserving property of the algorithm at stochastic
 97 quadrature points, which is one ingredient for ensuring hyperbolicity. However, one
 98 can go further in filtering. For example, recent work [26] utilizes a more sophisticated
 99 Lasso-regression-based filter to reduce oscillations of the numerical solution at shocks
 100 in the spatial domain.

101 In this work, we consider central-upwind scheme as an example of the under-
 102 lying numerical scheme for the stochastic shallow water equations. However, the
 103 main ideas developed in this work are independent of the particular choice of the
 104 numerical solver for hyperbolic problems and can be employed with various choices
 105 of the numerical schemes for hyperbolic problems. The central Nessyahu-Tadmor
 106 schemes, their generalization into higher resolution central schemes and semi-discrete
 107 central-upwind schemes are a class of robust Godunov-type Riemann problem-free
 108 projection-evolution methods for hyperbolic systems. They were originally developed
 109 in [30, 25, 22]. The family of central-upwind schemes has been successfully applied
 110 to problems in science and engineering, and in particular, to deterministic SWE and
 111 related models. A second-order central-upwind scheme was first extended to SWE
 112 in [20]. However, the scheme did not simultaneously satisfy the positivity-preserving
 113 and well-balanced properties. It was improved in [23] where the developed method
 114 captures the “lake-at-rest” steady state and preserves positivity of the water height.
 115 We refer the interested reader to [24, 21, 5, 6, 28, 19] for examples of other closely re-
 116 lated works. The numerical scheme developed in this work is mainly based on further
 117 extension to stochastic SWE of the framework proposed in [22, 23].

118 This paper is organized as follows. In [section 2](#), we introduce the stochastic SWE
 119 and the SG discretization of the system using a particular choice of the PCE for q^2/h .
 120 In [section 3](#), we discuss the hyperbolicity of the SG system obtained in [section 2](#) and
 121 present a sufficient condition to guarantee hyperbolicity of the SG SWE system. In
 122 [section 4](#), we present a well-balanced central-upwind scheme for the SG SWE model
 123 and derive a hyperbolicity-preserving CFL-type condition. In [section 5](#), we illustrate
 124 the robustness of the developed numerical scheme with several challenging tests.

125 **2. Modeling Stochastic Shallow Water Equations.** This section sets up
 126 the stochastic SWE problem and introduces notation used in this article.

127 **2.1. Stochastic modeling of the SWE.** We consider a complete probability
 128 space (Ω, \mathcal{F}, P) , with event space Ω , σ -algebra \mathcal{F} , and probability measure P . For
 129 $\omega \in \Omega$, a stochastic version of [\(1.1\)](#) is

$$130 \quad (2.1) \quad \begin{aligned} (h(x, t, \omega))_t + (q(x, t, \omega))_x &= 0, \\ (q(x, t, \omega))_t + \left(\frac{q^2(x, t, \omega)}{h(x, t, \omega)} + \frac{1}{2}gh^2(x, t, \omega) \right)_x &= -gh(x, t, \omega)B_x(x, \omega), \end{aligned}$$

131 where uncertainty enters the equation through, e.g., a stochastic model of the initial
 132 conditions or of the bottom topography B . Here, we present a stochastic model of the
 133 bottom topography. However, all our results generalize to other models of uncertainty

134 (e.g., in the initial conditions). We model B as a finite-dimensional random field,

135
$$B = B(x, \xi) = B_0(x) + \sum_{k=1}^d B_k(x) \xi_k,$$

 136

137 where $\xi = (\xi_1, \dots, \xi_d)$ is a d -dimensional random variable. Such a model can result, for
 138 example, from truncation of an infinite-dimensional Karhunen-Loéve decomposition.
 139 Under this model, the stochastic SWE model (2.1) can be written as a function of ξ ,

140 (2.2)
$$(h(x, t, \xi))_t + (q(x, t, \xi))_x = 0,$$

$$(q(x, t, \xi))_t + \left(\frac{q^2(x, t, \xi)}{h(x, t, \xi)} + \frac{1}{2} gh^2(x, t, \xi) \right)_x = -gh(x, t, \xi) B_x(x, \xi),$$

141 which, for the purposes of this paper, forms the continuous model problem for which
 142 we seek to compute numerical solutions.

143 **2.2. Polynomial chaos expansions.** We assume that the random variable ξ
 144 has a Lebesgue density $\rho : \mathbb{R}^d \rightarrow \mathbb{R}$. Polynomial chaos expansions (PCE) seek to
 145 approximate dependence on ξ by a polynomial function of ξ . With $\nu = (\nu_1, \dots, \nu_d) \in$
 146 \mathbb{N}_0^d a multi-index, then for $\zeta \in \mathbb{R}^d$ we adopt the standard notation,

147
$$\zeta^\nu := \prod_{j=1}^d \zeta_j^{\nu_j}, \quad \zeta^0 = \zeta^{(0,0,\dots,0)} = 1.$$

 148

149 We let $\Lambda \subset \mathbb{N}_0^d$ denote any non-empty, size- K finite set of multi-indices. We will
 150 assume throughout that $0 = (0, 0, \dots, 0) \in \Lambda$. Our PCE approximations will take
 151 place in a polynomial subspace defined by Λ :

152
$$P_\Lambda = \text{span}\{\zeta^\nu \mid \nu \in \Lambda\}, \quad \dim P_\Lambda = K := |\Lambda|.$$

154 We will also need “powers” of this set, defined by r -fold products of P_Λ elements:

155 (2.3)
$$P_\Lambda^r := \text{span} \left\{ \prod_{j=1}^r p_j \mid p_j \in P_\Lambda, j = 1, \dots, r \right\}, \quad \dim P_\Lambda^r \leq \binom{K}{r} = \binom{K+r-1}{r},$$

 156

157 where the dimension bound results from a combinatoric argument. Note that since
 158 $0 \in \Lambda$, then $P_\Lambda^r \subseteq P_\Lambda^s$ for any $r \leq s$. We will later exercise the notation above for $r = 3$.
 159 If ρ has finite polynomial moments of all orders, then there is an $L_\rho^2(\mathbb{R}^d)$ -orthonormal
 160 basis $\{\phi_k\}_{k=1}^\infty$ of P_Λ , i.e.,

161 (2.4)
$$\langle \phi_k, \phi_\ell \rangle_\rho := \int_{\mathbb{R}} \phi_k(s) \phi_\ell(s) \rho(s) ds = \delta_{k\ell}, \quad \phi_1(\xi) \equiv 1,$$

 162

163 for all $k, \ell \in \{1, \dots, K\}$, with the latter identification of ϕ_1 being an assumption we
 164 make without loss since $0 \in \Lambda$. If $y(x, t, \cdot) \in L_\rho^2(\mathbb{R})$, then under mild conditions on
 165 the probability measure ρ (see [13]) there exists a convergent expansion of y in these
 166 basis functions,

167
$$y(x, t, \cdot) \stackrel{L_\rho^2}{=} \sum_{k=1}^\infty \hat{y}_k(x, t) \phi_k(\cdot),$$

 168

169 where $\hat{y}_k(x, t)$ are (stochastic) Fourier coefficients in the basis $\{\phi_k\}_{k \in \mathbb{N}}$, and $\{\phi_\ell\}_{\ell > K}$
 170 are any $L_\rho^2(\mathbb{R}^d)$ -orthonormal basis for the orthogonal complement of P_Λ in the space of

171 all d -variate polynomials. A K -term P_Λ PCE *approximation* of the stochastic process
 172 y is then formed by truncating the summation above to terms in P_Λ :

173 (2.5)
$$y(x, t, \xi) \approx \sum_{k=1}^K \hat{y}_k(x, t) \phi_k(\xi) =: \mathcal{G}_\Lambda[y](x, t, \xi).$$

174 Above, we have defined the linear projection operator $\mathcal{G}_\Lambda : L^2_\rho \rightarrow P_\Lambda$.

175 **2.3. Operations on Truncated PCE Expansions.** Polynomial statistics of
 176 PCE expansions can be computed from a straightforward manipulation of their coef-
 177 ficients. For example,

178 (2.6)
$$\mathbb{E}[\mathcal{G}_\Lambda[y](x, t, \xi)] = \hat{y}_1(x, t), \quad \text{Var}[\mathcal{G}_\Lambda[y](x, t, \xi)] = \sum_{k=2}^K \hat{y}_k^2(x, t),$$

179 where \mathbb{E} is the expectation operator, and Var is the variance. In contrast, computing
 180 PCE expansions of nonlinear expressions is more complicated. To calculate the P_Λ -
 181 truncated PCE of the product of two stochastic processes $y(x, t, \xi)$ and $z(x, t, \xi)$, we
 182 introduce the notation

183 (2.7)
$$\mathcal{G}_\Lambda[y, z] := \mathcal{G}_\Lambda[\mathcal{G}_\Lambda[y] \mathcal{G}_\Lambda[z]] = \sum_{m=1}^K \left(\sum_{k, \ell=1}^K \hat{y}_k \hat{z}_\ell \langle \phi_k \phi_\ell, \phi_m \rangle_\rho \right) \phi_m(\xi).$$

185 The approximation above defines the *pseudo-spectral product*, which is a widely used
 186 strategy for computing PCE expansion products (e.g. [10][15]). The pseudo-spectral
 187 product is an exact projection onto P_Λ of the product of two P_Λ projections. Such an
 188 operation can be cast in linear algebraic terms by considering vectors comprised of
 189 the PCE expansion coefficients. Given $y \in P_\Lambda$, we will hereafter let $\hat{y} \in \mathbb{R}^K$ denote its
 190 ϕ_k -expansion coefficients. We now introduce the linear operator $\mathcal{P} : \mathbb{R}^K \rightarrow \mathbb{R}^{K \times K}$,

191 (2.8)
$$\mathcal{P}(\hat{y}) := \sum_{k=1}^K \hat{y}_k \mathcal{M}_k, \quad \mathcal{M}_k \in \mathbb{R}^{K \times K}, \quad (\mathcal{M}_k)_{\ell m} = \langle \phi_k, \phi_\ell \phi_m \rangle_\rho,$$

193 where \mathcal{M}_k is a symmetric matrix for each k . The following properties hold:

194 (2.9)
$$\mathcal{P}(\hat{y}) = (\mathcal{M}_1 \hat{y} | \mathcal{M}_2 \hat{y} | \cdots | \mathcal{M}_K \hat{y}), \quad \mathcal{P}(\hat{y}) \hat{z} = \mathcal{P}(\hat{z}) \hat{y}, \quad \widehat{\mathcal{G}_\Lambda[y, z]} = \mathcal{P}(\hat{y}) \hat{z},$$

196 where the last property is due to (2.7), and allows us to conclude the following.

197 **LEMMA 2.1.** *Let $a(\xi), b(\xi), c(\xi) \in P_\Lambda$ have ϕ_j -expansion coefficients $\hat{a}, \hat{b}, \hat{c} \in \mathbb{R}^K$,
 198 respectively. Then $\langle a, b c \rangle_\rho = \hat{a}^T \mathcal{P}(\hat{b}) \hat{c}$.*

199 *Proof.* Since $a \in P_\Lambda$, then

200
$$\langle a, b c \rangle_\rho = \langle b c, a \rangle_\rho = \langle \mathcal{G}_\Lambda[b, c], a \rangle_\rho = \hat{a}^T \widehat{\mathcal{G}_\Lambda[b, c]} \stackrel{(2.9)}{=} \hat{a}^T \mathcal{P}(\hat{b}) \hat{c}. \quad \square$$

202 We will also need to compute P_Λ truncations of ratios of processes (when for each
 203 (x, t) the denominator is a single-signed process with probability 1). We start by
 204 noting the following exact representation when y is a single-signed process:

205 (2.10)
$$\mathcal{G}_\Lambda \left[y \frac{z}{y} \right] (x, t, \xi) = \mathcal{G}_\Lambda[z](x, t, \xi).$$

206 We then use this to motivate the assumption,

207 (2.11)
$$\mathcal{G}_\Lambda \left[y, \frac{z}{y} \right] = \mathcal{G}_\Lambda[z] \stackrel{(2.9)}{\iff} \mathcal{P}(\hat{y}) \left(\widehat{\frac{z}{y}} \right) = \hat{z}.$$

208
209 This expression motivates the following definition for a new operator $\mathcal{G}_\Lambda^\dagger \left[\frac{z}{y} \right]$:

210 (2.12)
$$\mathcal{G}_\Lambda^\dagger \left[\frac{z}{y} \right] (\xi) := \sum_{k=1}^K c_k \phi_k(\xi),$$

211 where c_i is the i th element of $\widehat{\left(\frac{z}{y} \right)}$ defined by (2.11), assuming $\mathcal{P}(\hat{y})$ is invertible.

212 **2.4. Stochastic Galerkin Formulation for Shallow Water Equations.** We
213 start with (2.2) and perform a standard Galerkin procedure in stochastic (ξ) space
214 using polynomials from P_Λ . I.e., the first step is to replace h and q by the ansatz,

215 (2.13)
$$h \simeq h_\Lambda := \sum_{k=1}^K \hat{h}_j(x, t) \phi_j(\xi), \quad q \simeq q_\Lambda := \sum_{k=1}^K \hat{q}_j(x, t) \phi_j(\xi),$$

216
217 respectively, and B by $\mathcal{G}_\Lambda[B]$. Following this, we apply the projection operator \mathcal{G}_Λ to
218 both sides of (2.2) and insist on equality. However, in addition we make the following
219 crucial assumption about how we approximate the term q^2/h ,

220
221
$$\frac{q^2}{h} = \frac{q}{h} q \quad \longrightarrow \quad \mathcal{G}_\Lambda \left[\frac{q_\Lambda^2}{h_\Lambda} \right] = \mathcal{G}_\Lambda \left[q_\Lambda \mathcal{G}_\Lambda^\dagger \left[\frac{q_\Lambda}{h_\Lambda} \right] \right]$$

222 Performing these steps on (2.2) results in the system,

223 (2.14)
$$\frac{\partial}{\partial t} \left(\hat{h} \right) + \frac{\partial}{\partial x} \left(\frac{1}{2} g \mathcal{P}(\hat{h}) \hat{h} + \mathcal{P}(\hat{q}) \mathcal{P}^{-1}(\hat{h}) \hat{q} \right) = \begin{pmatrix} 0 \\ -g \mathcal{P}(\hat{h}) \hat{B}_x \end{pmatrix},$$

224 where \hat{h} and \hat{q} are each length- K vectors whose entries are the coefficients introduced
225 in (2.13). With $\hat{U} := (\hat{h}, \hat{q})^T$, and the flux and source terms

226 (2.15)
$$F(\hat{U}) = \begin{pmatrix} \hat{q} \\ \frac{1}{2} g \mathcal{P}(\hat{h}) \hat{h} + \mathcal{P}(\hat{q}) \mathcal{P}^{-1}(\hat{h}) \hat{q} \end{pmatrix}, \quad S(\hat{U}, \hat{B}) = \begin{pmatrix} 0 \\ -g \mathcal{P}(\hat{h}) \hat{B}_x \end{pmatrix},$$

227
228 then the system (2.14) can be written in general conservation law form,

229 (2.16)
$$\hat{U}_t + (F(\hat{U}))_x = S(\hat{U}, \hat{B}),$$

230 with flux Jacobian

231 (2.17)
$$J(\hat{U}) := \frac{\partial F}{\partial \hat{U}} = \begin{pmatrix} O & I \\ g \mathcal{P}(\hat{h}) - \mathcal{P}(\hat{q}) \mathcal{P}^{-1}(\hat{h}) \mathcal{P}(\hat{u}) & \mathcal{P}(\hat{u}) + \mathcal{P}(\hat{q}) \mathcal{P}^{-1}(\hat{h}) \end{pmatrix},$$

232 where we have introduced

233 (2.18)
$$\hat{u} = \mathcal{P}^{-1}(\hat{h}) \hat{q},$$

234 which can be viewed as the PCE coefficient vector of the velocity $u := \frac{q}{h}$. The
235 computation that gives the expression (2.17) for the Jacobian uses the property (2.9).
236 For more details, we refer interested readers to section 2.2 of [18].

237 We emphasize that (h, q) are the (x, t, ξ) -dependent solutions to the original sto-
238 chastic SWE equations (2.2), whereas (h_Λ, q_Λ) are the (x, t, ξ) -dependent solutions to
239 our SGSWE equations (2.16). In general, these two solutions are distinct. We first
240 articulate sufficient conditions under which (2.16) is a well-posed hyperbolic system.

241 **3. Hyperbolicity of The SG System.** In this section we show that the sys-
 242 tem (2.16) is hyperbolic under the condition that the matrix $\mathcal{P}(\hat{h})$ is positive definite.
 243 When there is no uncertainty, this condition reduces to $h > 0$, which ensures hyper-
 244 bolicity for the deterministic shallow water equations (1.1).

245 THEOREM 3.1. *If the matrix $\mathcal{P}(\hat{h})$ is strictly positive definite, the SG formulation
 246 (2.16) is hyperbolic.*

247 *Proof.* We will show that the Jacobian $\frac{\partial F}{\partial \hat{U}}$ is diagonalizable with real eigenvalues.
 248 Since $\mathcal{P}(\hat{h})$ is positive definite, then define

249 (3.1) $G := \sqrt{g\mathcal{P}(\hat{h})}, \quad A := gG^{-1}\mathcal{P}(\hat{q})G^{-1}, \quad B := \mathcal{P}(\hat{u}),$

251 where \sqrt{M} is the (unique) symmetric positive definite square root of a symmetric
 252 positive definite matrix M . Using these matrices, define

253 $P_1 := \begin{pmatrix} I & I \\ B+G & B-G \end{pmatrix}, \quad P_1^{-1} = \begin{pmatrix} 1 \\ -2 \end{pmatrix} \begin{pmatrix} G^{-1}B-I & -G^{-1} \\ -G^{-1}B-I & G^{-1} \end{pmatrix},$

255 where the formula for P_1^{-1} can be verified by direct computation. Then a calculation
 256 shows that

257 (3.2) $P_1^{-1} \frac{\partial F}{\partial \hat{U}} P_1 = -\frac{1}{2} \begin{pmatrix} -2G-B-A & A-B \\ A-B & 2G-B-A \end{pmatrix},$

259 which is symmetric. Thus $\frac{\partial F}{\partial \hat{U}}$ is similar to a diagonalizable matrix with real eigenval-
 260 ues, and so is itself real diagonalizable. \square

261 *Remark 3.2.* In the deterministic case, i.e, all the PCE coefficients are zero except
 262 possibly the very first coefficient and the matrix in (3.2) reduces to the eigenmatrix
 263 that symmetrizes the deterministic Jacobian matrix and a diagonal matrix.

264 For the deterministic SWE (1.1), the velocity u is bounded between the smallest
 265 and the largest eigenvalues of the Jacobian of the deterministic SWE. For the SG
 266 formulation (2.14), we have an analogous relation.

267 PROPOSITION 3.3. *The eigenvalues of the matrix $\mathcal{P}(\hat{u})$ are bounded between the
 268 smallest and the largest eigenvalues of the Jacobian matrix $J(\hat{U})$, i.e.,*

269 (3.3) $\lambda_{\max}(J(\hat{U})) \geq \lambda_{\max}(\mathcal{P}(\hat{u})) \geq \lambda_{\min}(\mathcal{P}(\hat{u})) \geq \lambda_{\min}(J(\hat{U})).$

270 *Proof.* By the proof of Theorem 3.1, the matrix $J(\hat{U})$ is similar to the sym-
 271 metric matrix $D := P_1^{-1} \frac{\partial F}{\partial \hat{U}} P_1$ defined in (3.2). For an arbitrary unit vector $\hat{y} =$
 272 $(\hat{y}_1, \hat{y}_2, \dots, \hat{y}_K)^T \in \mathbb{R}^K$, then $\hat{z} := \frac{1}{\sqrt{2}}[\hat{y}^T, \hat{y}^T]^T \in \mathbb{R}^{2K}$ is also a unit vector. Then,

273 (3.4) $\hat{z}^T D \hat{z} = \hat{y}^T \mathcal{P}(\hat{u}) \hat{y}.$

274 From the above relation, and using properties of the Rayleigh quotient for $\mathcal{P}(\hat{u})$,

275 $\lambda_{\max}(\mathcal{P}(\hat{u})) \geq \hat{z}^T D \hat{z} \geq \lambda_{\min}(\mathcal{P}(\hat{u})),$

276 where equalities can be achieved by proper selections of \hat{y} . Using similar Rayleigh
 277 quotient properties for D and noting that \hat{z} ranges over a subset of \mathbb{R}^{2K} , then

278 (3.5) $\lambda_{\max}(D) \geq \lambda_{\max}(\mathcal{P}(\hat{u})) \geq \lambda_{\min}(\mathcal{P}(\hat{u})) \geq \lambda_{\min}(D)$

279 The inequalities (3.3) follow since D is similar to $J(\hat{U})$. \square

280 In the deterministic SWE, positivity of the water height h ensures hyperbolicity
 281 of the PDE system. [Theorem 3.1](#) shows that the stochastic variant of the positivity
 282 condition is that $\mathcal{P}(\hat{h})$ is positive definite. Much of the rest of this paper is devoted
 283 to deriving numerical procedures to guarantee this condition.

284 **3.1. Positive definiteness of $\mathcal{P}(\hat{h})$.** In this subsection, we present a computa-
 285 tionally convenient sufficient condition that guarantees $\mathcal{P}(\hat{h}) > 0$, and hence guaran-
 286 tees hyperbolicity.

287 **THEOREM 3.4.** *Given Λ , let nodes ξ_m and weights τ_m satisfying $\{(\xi_m, \tau_m)\}_{m=1}^M \subset$
 288 $\mathbb{R}^d \times (0, \infty)$ represent any M -point positive quadrature rule that is exact on P_Λ^3 , i.e.,*

$$289 \quad (3.6) \quad \int_{\mathbb{R}^d} p(\xi) \rho(\xi) d\xi = \sum_{m=1}^M p(\xi_m) \tau_m, \quad p \in P_\Lambda^3.$$

291 *If*

$$293 \quad (3.7) \quad h_\Lambda(x, t, \xi_m) > 0 \quad \forall m = 1, \dots, M,$$

294 *then the SGSWE system (2.16) is hyperbolic.*

295 *Proof.* We will show that (3.7) implies $\mathcal{P}(\hat{h}) > 0$, which in turn ensures hyperbolicity from [Theorem 3.1](#). Let $\hat{z} = (\hat{z}_k)_{k=1}^K$ be any nontrivial vector in \mathbb{R}^K , and define its associated P_Λ polynomial $z(\xi) := \sum_{k=1}^K \hat{z}_k \phi_k(\xi) \neq 0$. Then $z(\xi)$ cannot vanish at all quadrature points simultaneously since if it did we obtain the contradiction,

$$299 \quad 0 \neq \|\hat{z}\|^2 = \langle z, z \rangle_\rho \stackrel{(3.6)}{=} \sum_{j=1}^M z^2(\xi_j) \tau_j = 0,$$

300 where we have used the fact that $P_\Lambda^2 \subseteq P_\Lambda^3$ to utilize (3.6). Then since the quadrature
 301 rule is positive and (3.7) holds, we have

$$302 \quad 0 < \sum_{j=1}^M h_\Lambda(x, t, \xi_j) z^2(\xi_j) \tau_j \stackrel{(3.6)}{=} \langle h_\Lambda(x, t, \xi), z^2(\xi) \rangle \stackrel{\text{Lemma (2.1)}}{=} \hat{z}^T \mathcal{P}(\hat{h}) \hat{z},$$

304 establishing that $\mathcal{P}(\hat{h})$ is positive definite. \square

305 Thus, by guaranteeing positivity of h_Λ at a finite number of points, we can ensure
 306 hyperbolicity of the SGSWE system. For arbitrary stochastic dimension d and poly-
 307 nomial space P_Λ , there is a worst-case upper bound on the size of this finite set.

308 **COROLLARY 3.5.** *There is some $M \leq \dim P_\Lambda^3 \leq \frac{K(K+1)(K+2)}{6}$ such that the dis-
 309 crete pointwise positivity condition (3.7) guarantees hyperbolicity of (2.16).*

310 We give the proof in [Lemma B.2](#) in the Appendix. One might consider the somewhat
 311 simpler condition of restricting $\hat{h}_1 > 0$ for hyperbolicity since \hat{h}_1 is the expected value
 312 of h_Λ . This condition is actually implied by the condition in [Theorem 3.4](#).

313 **COROLLARY 3.6.** *If the conditions of [Theorem 3.4](#) are satisfied, then $\hat{h}_1 > 0$.*

314 *Proof.* Since $\tau_j > 0$ and $h_\Lambda > 0$ at the quadrature points, then

$$315 \quad \hat{h}_1 = \int_{\mathbb{R}^d} h_\Lambda(x, t, \zeta) \rho(\zeta) d\zeta = \sum_{j=1}^M h_\Lambda(x, t, \xi_j) \tau_j > 0, \quad \square$$

317 A computable condition ensuring hyperbolicity therefore requires a positive quadrature rule that is exact on P_Λ^3 . For general densities ρ over \mathbb{R}^d , computing such a quadrature rule is a very difficult task. But this is possible in specialized cases.

320 For example, if $d = 1$ and $\Lambda = \{0, 1, \dots, K - 1\}$, then an optimal choice of 321 positive quadrature is the ρ -Gaussian quadrature. Since $P_\Lambda^3 = \text{span}\{1, \zeta, \dots, \zeta^{3K-3}\}$, 322 then choosing the positive M -point Gaussian quadrature,

$$323 \quad \{\xi_m\}_{m=1}^M = \phi_{M+1}^{-1}(0), \quad \tau_m = \frac{1}{\sum_{j=1}^M \phi_j^2(\xi_m)},$$

325 with $M \geq \lceil \frac{3K}{2} \rceil - 1$ satisfies the conditions of [Theorem 3.4](#) (and does so with substantially 326 fewer points than the $\sim K^3/6$ worst-case bound from [Corollary 3.5](#)). Gaussian 327 quadrature rules have real-valued nodes and positive weights [38].

328 In spaces with $d > 1$, if ρ is tensorial, then tensorizing Gauss quadrature rules 329 achieves similar results. I.e., assume

$$330 \quad \rho(\xi) = \prod_{J=1}^d \rho_J(\xi_J), \quad \xi \in \mathbb{R}^d,$$

332 We can always enclose P_Λ within a tensor-product polynomial space:

$$333 \quad P_\Lambda^3 \subseteq P_{3k, \infty} := \{\lambda \in \mathbb{N}_0^d \mid \lambda_J \leq 3\kappa_J \text{ for } J = 1, \dots, d\}, \quad \kappa_J := \max_{\nu \in \Lambda} \nu_J.$$

335 For a fixed $J \in \{1, \dots, d\}$, let $\{(\xi_{m, M_J}^{(J)}, \tau_{m, M_J}^{(J)})\}_{m=1}^{M_J}$ denote the $M_J := (\lceil \frac{3\kappa_J}{2} \rceil - 1)$ - 336 point ρ_J -Gaussian quadrature rule on \mathbb{R} . Then the tensorization of these d univariate 337 quadrature rules results in an $M := (\prod_{J=1}^d M_J)$ -point positive quadrature rule that 338 is exact on $P_{3k, \infty}$, hence on P_Λ^3 , and thus satisfies the conditions of [Theorem 3.4](#).

339 **4. Numerical Scheme for Stochastic Shallow Water Equations.** In this 340 section, we derive a well-balanced central-upwind scheme that preserves the hyper- 341 bolicity of the SG formulation (2.16) at every time step.

342 **4.1. Central-Upwind Scheme for the SG System.** We first introduce the 343 central-upwind scheme for the SG system (2.16). [Appendix A](#) provides a brief 344 summary of the second-order central-upwind schemes for balance laws. With $\{\mathcal{C}_i\}_{i=1}^N$ a 345 partition of a bounded closed interval, let $x_{i \pm \frac{1}{2}}$ denote the partition boundaries, and 346 define the cell average of the vector \hat{U} over the i th cell $\mathcal{C}_i =: [x_{i-\frac{1}{2}}, x_{i+\frac{1}{2}}]$ as,

$$\bar{\mathbf{U}}_i(t) := \begin{pmatrix} \bar{\mathbf{h}}_i(t) \\ \bar{\mathbf{q}}_i(t) \end{pmatrix} := \frac{1}{\Delta x} \int_{\mathcal{C}_i} \begin{pmatrix} \hat{h}(x, t) \\ \hat{q}(x, t) \end{pmatrix} dx \in \mathbb{R}^{2K}.$$

342 We have introduced notation for common quantities in finite volume-type schemes. 343 While \hat{U}_k is the k th component of the vector \hat{U} , the bold letter \mathbf{U} with subscripts and 344 superscripts is used here to introduce the cell averages and pointwise reconstructions, 345 respectively, of the vector $\hat{U}(x, t)$. I.e., $\mathbf{U}_{i+\frac{1}{2}}^-$ is the approximated value of \hat{U} at the left- 346 hand side of spatial location $x = x_{i+\frac{1}{2}}$, which is reconstructed from the cell averages 347 $\bar{\mathbf{U}}_i$. A similar reasoning applies to $(\mathbf{h}, \hat{h}, \hat{h}_k)$ and $(\mathbf{q}, \hat{q}, \hat{q}_k)$. To minimize clutter, we will 348 notationally suppress t dependence from here onward. The possible discontinuities of

349 the system (2.16) at the cell interface $x = x_{i+\frac{1}{2}}$, where $\mathcal{C}_i = [x_{i-\frac{1}{2}}, x_{i+\frac{1}{2}}]$, propagates
 350 with left- and right-sided local speeds that can be estimated by,

351 (4.1)
$$\begin{aligned} a_{i+\frac{1}{2}}^- &= \min \left\{ \lambda_1 \left(J(\mathbf{U}_{i+\frac{1}{2}}^-) \right), \lambda_1 \left(J(\mathbf{U}_{i+\frac{1}{2}}^+) \right), 0 \right\}, \\ a_{i+\frac{1}{2}}^+ &= \max \left\{ \lambda_{2K} \left(J(\mathbf{U}_{i+\frac{1}{2}}^-) \right), \lambda_{2K} \left(J(\mathbf{U}_{i+\frac{1}{2}}^+) \right), 0 \right\}, \end{aligned}$$

352 where $\lambda_1 \leq \lambda_2 \leq \dots \leq \lambda_{2K}$ are the eigenvalues of the $J(\cdot)$ in (2.17), and $\mathbf{U}_{i+\frac{1}{2}}^-$
 353 and $\mathbf{U}_{i+\frac{1}{2}}^+$ are the left- and right-sided pointwise reconstructions in the i th cell. The
 354 semi-discrete form of the central-upwind scheme for the SG system (2.16) reads as,

355 (4.2)
$$\frac{d}{dt} \bar{\mathbf{U}}_i = -\frac{\mathcal{F}_{i+\frac{1}{2}} - \mathcal{F}_{i-\frac{1}{2}}}{\Delta x} + \bar{\mathbf{S}}_i, \quad \bar{\mathbf{S}}_i \approx \frac{1}{\Delta x} \int_{\mathcal{C}_i} S(\mathbf{U}, \mathbf{B}) dx$$

357 with $\bar{\mathbf{S}}_i$ a well-balanced discretization of the source term, which we discuss below.
 358 With F the flux term in (2.15), the numerical flux \mathcal{F} is given by

359 (4.3)
$$\mathcal{F}_{i+\frac{1}{2}} := \frac{a_{i+\frac{1}{2}}^+ F(\mathbf{U}_{i+\frac{1}{2}}^-) - a_{i+\frac{1}{2}}^- F(\mathbf{U}_{i+\frac{1}{2}}^+)}{a_{i+\frac{1}{2}}^+ - a_{i+\frac{1}{2}}^-} + \frac{a_{i+\frac{1}{2}}^+ a_{i+\frac{1}{2}}^-}{a_{i+\frac{1}{2}}^+ - a_{i+\frac{1}{2}}^-} \left[\mathbf{U}_{i+\frac{1}{2}}^+ - \mathbf{U}_{i+\frac{1}{2}}^- \right].$$

360 **4.2. Well-Balanced Property.** In applications of the deterministic SWE, sim-
 361 ulations should accurately capture the so-called “lake-at-rest” steady state solution,
 362 or small perturbations of the lake-at-rest steady state. A *well-balanced* numerical
 363 scheme for the SWE captures the lake-at-rest solution exactly at discrete level. An
 364 analogous lake-at-rest state for the stochastic shallow water equations (2.14) is

365 (4.4)
$$q_\Lambda(x, t, \xi) \equiv 0, \quad h_\Lambda + \mathcal{G}_\Lambda[B](x, t, \xi) \equiv C(\xi),$$

366 where $C(\xi)$ depends only on ξ . This solution corresponds to still water with a flat
 367 stochastic water surface. Equation (4.4) can be rewritten in the vector form,

368 (4.5)
$$\hat{q} \equiv \mathbf{0}, \quad \hat{h} + \hat{\mathbf{B}} \equiv \hat{C}.$$

369 In order to derive a well-balanced central upwind scheme for the SGSWE, we first
 370 replace the original bottom function $\hat{\mathbf{B}}$ by its continuous linear interpolant. At every
 371 time step, we compute the PCE vector for the cell averages of the water surface by
 372 $\bar{\mathbf{w}}_i := \bar{\mathbf{h}}_i + \bar{\mathbf{B}}_i$ and the pointwise reconstructions of the water surface by $\mathbf{w}_{i+\frac{1}{2}}^\pm$ using
 373 a generalized minmod limiter (see Appendix A). The pointwise reconstructions of the
 374 water height are then computed by

375 (4.6)
$$\mathbf{h}_{i+\frac{1}{2}}^\pm := \mathbf{w}_{i+\frac{1}{2}}^\pm - \mathbf{B}_{i+\frac{1}{2}},$$

377 where $\mathbf{B}_{i+\frac{1}{2}}$ is the PCE vector for $\mathcal{G}_\Lambda[B(x_{i+\frac{1}{2}}, t, \xi)]$. The numerical fluxes $\{\mathcal{F}_{i+\frac{1}{2}}\}_{i=1}^N$
 378 are subsequently computed using the reconstructed PCE of the water height defined
 379 in (4.6). After that, the well-balanced property of the scheme is ensured by a special
 380 choice of the source term $\bar{\mathbf{S}}_i$.

381 **LEMMA 4.1.** *With $\mathbf{B}_{i\pm\frac{1}{2}}$ the PCE vectors for $\mathcal{G}_\Lambda[B(x_{i\pm\frac{1}{2}}, t, \xi)]$,*
 382 *if we choose*

383 (4.7)
$$\bar{\mathbf{S}}_i := \begin{pmatrix} \mathbf{0} \\ -\frac{1}{\Delta x} g \mathcal{P}(\bar{\mathbf{h}}_i) (\mathbf{B}_{i+\frac{1}{2}} - \mathbf{B}_{i-\frac{1}{2}}) \end{pmatrix},$$

384 *then the central-upwind scheme (4.2) satisfies the well-balanced property.*

385 *Proof.* We have $\bar{\mathbf{B}}_i = (\mathbf{B}_{i+\frac{1}{2}} + \mathbf{B}_{i-\frac{1}{2}})/2$, and the cell average PCE vector of the
 386 water surface $\bar{\mathbf{w}}_i := \bar{\mathbf{h}}_i + \bar{\mathbf{B}}_i$. Let the pointwise reconstructions for water surface be
 387 $\mathbf{w}_{i+\frac{1}{2}}^\pm$. Assume that at time t , the stochastic water surface is flat and the water is
 388 still, i.e., $\bar{\mathbf{w}}_i \equiv \mathbf{w}^*$ is a constant vector for all i , and $\bar{\mathbf{q}}_i \equiv \mathbf{0}$. Then a second-order
 389 piecewise linear reconstruction procedure produces $\mathbf{w}_{i+\frac{1}{2}}^\pm \equiv \mathbf{w}^*$ and $\mathbf{q}_{i+\frac{1}{2}}^\pm \equiv \mathbf{0}$. Hence,
 390 the numerical flux defined in (4.3) becomes,

391 (4.8)
$$\mathcal{F}_{i+\frac{1}{2}} = \begin{pmatrix} \mathbf{0} \\ \frac{g}{2} \mathcal{P}(\mathbf{w}^* - \mathbf{B}_{i+\frac{1}{2}})(\mathbf{w}^* - \mathbf{B}_{i+\frac{1}{2}}) \end{pmatrix} =: \begin{pmatrix} \mathcal{F}_{i+\frac{1}{2}}^h \\ \mathcal{F}_{i+\frac{1}{2}}^q \end{pmatrix}.$$

392 Then with $\bar{\mathbf{S}}_i = (\bar{\mathbf{S}}_{i,1}^T, \bar{\mathbf{S}}_{i,2}^T)^T$, the corresponding semidiscrete form is

393 (4.9)
$$\begin{aligned} \frac{d}{dt} \bar{\mathbf{h}}_i &= \bar{\mathbf{S}}_{i,1} \\ \frac{d}{dt} \bar{\mathbf{q}}_i &= -\frac{1}{\Delta x} \frac{g}{2} \left[\mathcal{P}(\mathbf{w}^* - \mathbf{B}_{i+\frac{1}{2}})(\mathbf{w}^* - \mathbf{B}_{i+\frac{1}{2}}) - \mathcal{P}(\mathbf{w}^* - \mathbf{B}_{i-\frac{1}{2}})(\mathbf{w}^* - \mathbf{B}_{i-\frac{1}{2}}) \right] + \bar{\mathbf{S}}_{i,2} \end{aligned}.$$

394 To balance these equations, we choose $\bar{\mathbf{S}}_{i,1}$ and $\bar{\mathbf{S}}_{i,2}$ so that the right-hand side
 395 vanishes. Clearly we need $\bar{\mathbf{S}}_{i,1} \equiv \mathbf{0}$. To simplify the computation for $\bar{\mathbf{S}}_{i,2}$, let $\Delta \mathbf{B}_i =$
 396 $\mathbf{B}_{i+\frac{1}{2}} - \mathbf{B}_{i-\frac{1}{2}}$, then $\bar{\mathbf{B}}_i = \mathbf{B}_{i+\frac{1}{2}} - \frac{1}{2} \Delta \mathbf{B}_i = \mathbf{B}_{i-\frac{1}{2}} + \frac{1}{2} \Delta \mathbf{B}_i$. By linearity of the operator
 397 \mathcal{P} and the property (2.9),

398 (4.10)
$$\begin{aligned} \bar{\mathbf{S}}_{i,2} &= \frac{1}{\Delta x} \frac{g}{2} \left[\mathcal{P}(\mathbf{w}^* - \mathbf{B}_{i+\frac{1}{2}})(\mathbf{w}^* - \mathbf{B}_{i+\frac{1}{2}}) - \mathcal{P}(\mathbf{w}^* - \mathbf{B}_{i-\frac{1}{2}})(\mathbf{w}^* - \mathbf{B}_{i-\frac{1}{2}}) \right] \\ &= \frac{1}{\Delta x} \frac{g}{2} \left[\mathcal{P} \left(\mathbf{w}^* - \bar{\mathbf{B}}_i - \frac{1}{2} \Delta \mathbf{B}_i \right) \left(\mathbf{w}^* - \bar{\mathbf{B}}_i - \frac{1}{2} \Delta \mathbf{B}_i \right) \right. \\ &\quad \left. - \mathcal{P} \left(\mathbf{w}^* - \bar{\mathbf{B}}_i + \frac{1}{2} \Delta \mathbf{B}_i \right) \left(\mathbf{w}^* - \bar{\mathbf{B}}_i + \frac{1}{2} \Delta \mathbf{B}_i \right) \right] \quad \square \\ &= \frac{1}{\Delta x} \frac{g}{2} \left[\mathcal{P}(\mathbf{w}^* - \bar{\mathbf{B}}_i) (-\Delta \mathbf{B}_i) - \mathcal{P} \left(\frac{\Delta \mathbf{B}_i}{2} \right) (2\mathbf{w}^* - 2\bar{\mathbf{B}}_i) \right] \\ &= -g \mathcal{P}(\mathbf{w}^* - \bar{\mathbf{B}}_i) \left(\frac{\mathbf{B}_{i+\frac{1}{2}} - \mathbf{B}_{i-\frac{1}{2}}}{\Delta x} \right) = -g \mathcal{P}(\bar{\mathbf{h}}_i) \left(\frac{\mathbf{B}_{i+\frac{1}{2}} - \mathbf{B}_{i-\frac{1}{2}}}{\Delta x} \right). \end{aligned}$$

399 In the meantime, (4.7) reduces to the deterministic well-balanced quadrature ap-
 400 proximation when there is no uncertainty. The deterministic formula is obtained by
 401 applying the midpoint quadrature rule to the cell averages (4.2) with the derivative
 402 term $\mathbf{B}_x(x_i)$ approximated by the finite difference $(\mathbf{B}_{i+\frac{1}{2}} - \mathbf{B}_{i-\frac{1}{2}})/\Delta x$ [23].

403 **4.3. Hyperbolicity-Preserving CFL-type conditions.** To determine
 404 hyperbolicity-preserving CFL-type conditions, we focus on the first K equations in
 405 (4.2) which prescribe evolution of $\bar{\mathbf{h}}_i$,

406 (4.11)
$$\frac{d}{dt} \bar{\mathbf{h}}_i = -\frac{1}{\Delta x} \left[\mathcal{F}_{i+\frac{1}{2}}^h(t) - \mathcal{F}_{i-\frac{1}{2}}^h(t) \right],$$

407 where

408 (4.12)
$$\mathcal{F}_{i+\frac{1}{2}}^h = \frac{a_{i+\frac{1}{2}}^+ \mathbf{q}_{i+\frac{1}{2}}^- - a_{i+\frac{1}{2}}^- \mathbf{q}_{i+\frac{1}{2}}^+}{a_{i+\frac{1}{2}}^+ - a_{i+\frac{1}{2}}^-} + \frac{a_{i+\frac{1}{2}}^+ a_{i+\frac{1}{2}}^-}{a_{i+\frac{1}{2}}^+ - a_{i+\frac{1}{2}}^-} \left[\mathbf{h}_{i+\frac{1}{2}}^+ - \mathbf{h}_{i+\frac{1}{2}}^- \right].$$

409 A fully discrete version of (4.11) computes the unknowns at fixed values of time, t^n ,
410 $n \in \mathbb{N}_0$, with $t^n < t^{n+1}$. For example, with $\bar{\mathbf{h}}_i^n$ the numerical approximation to $\bar{\mathbf{h}}_i(t^n)$,
411 and $\Delta t^n := t^{n+1} - t^n$, the Forward Euler discretization of (4.11) reads,

412 (4.13)
$$\bar{\mathbf{h}}_i^{n+1} = \bar{\mathbf{h}}_i^n - \lambda_i^n \left[\mathcal{F}_{i+\frac{1}{2}}^{\hat{h}}(t^n) - \mathcal{F}_{i-\frac{1}{2}}^{\hat{h}}(t^n) \right], \quad \lambda_i^n := \frac{\Delta t^n}{\Delta x_i}.$$

414 The following CFL condition guarantees hyperbolicity of the system (4.13) at $t = t^{n+1}$
415 for all cell averages, by enforcing the positivity condition prescribed in [Theorem 3.4](#).

416 **LEMMA 4.2.** *Let $\{\xi_j\}_{j=1}^M$ be the nodes of a quadrature rule satisfying the condi-
417 tions of [Theorem 3.4](#). Assume that $\bar{\mathbf{h}}_i^n(\xi_j) > 0$ for $1 \leq j \leq M$. If Δt^n satisfies*

418 (4.14)
$$\Delta t^n < \Delta t_h^n := \min_{\substack{1 \leq j \leq M \\ i}} \left\{ \Delta x_i \left| \frac{(\bar{\mathbf{h}}_i^n)^T \Phi(\xi_j)}{\left[\mathcal{F}_{i+\frac{1}{2}}^{\hat{h}}(t_n) - \mathcal{F}_{i-\frac{1}{2}}^{\hat{h}}(t_n) \right]^T \Phi(\xi_j)} \right| \right\},$$

420 then the flux Jacobian (2.17), $J(\bar{\mathbf{U}}_i^{n+1})$ is diagonalizable with real eigenvalues.

421 *Proof.* [Theorem 3.4](#) guarantees the conclusion if $\bar{\mathbf{h}}_i^{n+1}(\xi_j) > 0$, for $1 \leq j \leq M$, so
422 we proceed to show this latter property. For each j , the inequality

423 (4.15)
$$0 < (\bar{\mathbf{h}}_i^{n+1})^T \Phi(\xi_j) = (\bar{\mathbf{h}}_i^n)^T \Phi(\xi_j) - \lambda_i^n \left[\mathcal{F}_{i+\frac{1}{2}}^{\hat{h}}(t_n) - \mathcal{F}_{i-\frac{1}{2}}^{\hat{h}}(t_n) \right]^T \Phi(\xi_j)$$

425 holds if we choose

426
$$\frac{\Delta t^n}{\Delta x_i} = \lambda_i^n < \min_{\substack{1 \leq j \leq M}} \left\{ \left| \frac{(\bar{\mathbf{h}}_i^n)^T \Phi(\xi_j)}{\left[\mathcal{F}_{i+\frac{1}{2}}^{\hat{h}}(t_n) - \mathcal{F}_{i-\frac{1}{2}}^{\hat{h}}(t_n) \right]^T \Phi(\xi_j)} \right| \right\}. \quad \square$$

428 Multiplying both sides by Δx_i and minimizing over i yields the conclusion.

429 The condition (4.14) ensures positivity of the water height, but we also need to
430 adhere to standard wavespeed-based CFL stability conditions. Thus, we will choose

431 (4.16)
$$\Delta t^n = 0.9 \min \left\{ \Delta t_h^n, \min_i \frac{\Delta x_i}{\max\{a_{i+\frac{1}{2}}^+, -a_{i+\frac{1}{2}}^-\}} \right\}.$$

432 To extend these conditions to hold higher-order schemes, we use strong stability-
433 preserving Runge-Kutta schemes [16] to solve the semidiscrete system (4.2). The
434 analysis above for the condition (4.14) still holds for this solver since the ODE solver
435 can be written as a convex combination of several forward Euler steps. However, an
436 adaptive time-step control needs to be adopted to determine the time step [6, 19].
437 The analysis above can also be naturally extended to any other finite volume solvers.

438 *Remark 4.3.* The CFL condition (4.14) can be relaxed if the signs of the fluxes
439 are taken into account in the inequality (4.15). In implementation, this can be used
440 to reduce the simulation time.

441 It is important to note that, the CFL-type condition provided above is limited
442 to the cell averages. For the second-order (or higher-order) central-upwind scheme,
443 additional correction is required for the pointwise reconstructions $\mathbf{U}_{i+\frac{1}{2}}^\pm$ to ensure
444 hyperbolicity of (4.13). Similarly, special correction is needed for the near-dry states,
445 where the matrices $\mathcal{P}(\mathbf{h}_{i+\frac{1}{2}}^\pm)$ are close to singular, to ensure hyperbolicity.

446 **4.3.1. Hyperbolicity-Preserving Correction to the Reconstruction.** As
447 suming $(\bar{\mathbf{h}}_i^n)^T \Phi(\xi_j) > 0$, we are able to enforce $(\bar{\mathbf{h}}_i^{n+1})^T \Phi(\xi_j) > 0$ for $j = 1, \dots, M$
448 under the CFL-type condition (4.16), see Lemma 4.2. However, the one-sided propa-
449 gation speeds (4.1) in the central-upwind scheme (4.13) are estimated by the eigenval-
450 ues of the Jacobian $\frac{\partial F}{\partial \tilde{U}}$ using the pointwise values at the cell interfaces. Thus, compu-
451 tation of these wave speeds requires positivity of the pointwise reconstruction at quad-
452 rature points, i.e., $(\mathbf{h}_{i \mp \frac{1}{2}}^\pm)^T \Phi(\xi_j) > 0$, which is not guaranteed by $(\bar{\mathbf{h}}_i^n)^T \Phi(\xi_j) > 0$.
453 To resolve this problem, we use the filtering strategy proposed in [36] to filter $\mathbf{h}_{i \mp \frac{1}{2}}^\pm$.

454 Given a polynomial $p_{\hat{y}}(\xi) = \sum_{k=1}^K \hat{y}_k \phi_k(\xi)$ with positive moment \hat{y}_1 , we find the
455 smallest possible weight μ' such that the weighted averages of the polynomial $p_{\hat{y}}(\xi)$
456 and the moment \hat{y}_1 are nonnegative at given quadrature points $\{\xi_j\}_{j=1}^M$, i.e.,

457 (4.17)
$$\mu' \hat{y}_1 + (1 - \mu') p_{\hat{y}}(\xi) \geq 0 \Leftrightarrow \hat{y}_1 + \sum_{k=2}^K (1 - \mu') \hat{y}_k \phi_k(\xi_j) \geq 0, j = 1, \dots, M,$$

458 and the coefficients of the polynomial are filtered by

459 (4.18)
$$\hat{y}_1 = \hat{y}_1, \quad \hat{y}_k = (1 - \mu) \hat{y}_k, k = 2, \dots, K,$$

460 where $\mu = \min\{\mu' + \delta, 1\}$, and we select $\delta = 10^{-10}$ in our scheme. Hence, the filtered
461 polynomial $p_{\hat{y}}(\xi) = \sum_{k=1}^K \hat{y}_k \phi_k(\xi)$ is positive at given quadrature points $\{\xi_j\}_{j=1}^M$. We
462 filter $p_{\hat{y}}(\xi) = \sum_{k=1}^K \hat{y}_k \phi_k(\xi)$ and $p_{\hat{z}}(\xi) = \sum_{k=1}^K \hat{z}_k \phi_k(\xi)$ simultaneously by calculating
463 the individual filtering parameters $\mu'_{\hat{y}}$ and $\mu'_{\hat{z}}$ for $p_{\hat{y}}(\xi)$ and $p_{\hat{z}}(\xi)$, respectively, through
464 (4.17). Then the simultaneous filtering parameter is set to $\mu = \min\{\mu'_{\hat{y}} + \delta, \mu'_{\hat{z}} + \delta, 1\}$.

465 We will exercise the filtering strategy (4.17)-(4.18) for pointwise reconstructions.
466 We compute the filtering parameter μ_i^n at time $t = t^n$ for the i th cell for $(\mathbf{h}_{i \mp \frac{1}{2}}^\pm)^T \Phi(\xi)$
468 according to (4.17). The pointwise reconstructions $\mathbf{h}_{i \mp \frac{1}{2}}^\pm$ are then filtered by

469 (4.19)
$$\left(\mathbf{h}_{i \mp \frac{1}{2}}^\pm \right)_1 = \left(\mathbf{h}_{i \mp \frac{1}{2}}^\pm \right)_1, \quad \left(\mathbf{h}_{i \mp \frac{1}{2}}^\pm \right)_k = (1 - \mu_i^n) \left(\mathbf{h}_{i \mp \frac{1}{2}}^\pm \right)_k, k = 2, \dots, K.$$

470 The corresponding cell average is adjusted accordingly in order to remain consistent,

471 (4.20)
$$\bar{\mathbf{h}}_i^n = \frac{1}{2} \left(\mathbf{h}_{i-\frac{1}{2}}^+ + \mathbf{h}_{i+\frac{1}{2}}^- \right).$$

472

473 *Remark 4.4.* To reduce oscillations in $q_\Lambda(x, t, \xi)$, we can also filter the discharge
474 reconstructions $\mathbf{q}_{i-\frac{1}{2}}^\pm$. The corresponding cell average needs to be adjusted similarly
475 to (4.20). In subsection 5.3 when $(\alpha, \beta) = (1, 3)$, we adopt this filtering approach to
476 reduce oscillations in the discharge.

477 As an alternative to the filtering above, one can use a convex-optimization based
478 method [4] to enforce the positivity of $(\mathbf{h}_{i \mp \frac{1}{2}}^\pm)^T \Phi(\xi)$ at quadrature points $\{\xi_j\}_{j=1}^M$.

479 **4.3.2. Near-Dry State Correction.** When the polynomial $(\bar{\mathbf{h}}_i^n)^T \Phi(\xi) \sim 0$,
480 two issues related to the dry state may occur. One is that the first moments of the
481 polynomials $(\mathbf{h}_{i \mp \frac{1}{2}}^\pm)^T \Phi(\xi)$ may become nonpositive. This can happen even when the
482 system is deterministic [23]. Nonpositive first moments may lead to the failure of the

483 filtering correction (4.17)-(4.18). In our scheme, we adopt the following correction for
 484 nonpositive first moments. Denote the first moments of $\mathbf{h}_{i \mp \frac{1}{2}}^\pm$ by $(\mathbf{h}_{i \mp \frac{1}{2}}^\pm)_1$, then

485 (4.21)
$$\text{if } (\mathbf{h}_{i \mp \frac{1}{2}}^\pm)_1 \leq 0 \text{ then take } \mathbf{h}_{i \mp \frac{1}{2}}^\pm = \mathbf{0}, \quad \mathbf{h}_{i \mp \frac{1}{2}}^\mp = 2\bar{\mathbf{h}}_i^n.$$

487 Note that, this strategy reduces to a similar correction in the central-upwind scheme
 488 for the deterministic shallow water equations [23].

Another issue may happen when the matrix $\mathcal{P}(\mathbf{h}_{i+\frac{1}{2}}^+)$ or $\mathcal{P}(\mathbf{h}_{i+\frac{1}{2}}^-)$ is ill-conditioned, which may lead to problems with round-off errors when solving the corresponding linear system (2.18). To resolve this issue, we extend to the stochastic model the desingularization process for the deterministic problem [23, 19]. We demonstrate our correction using the matrix $\mathcal{P}(\mathbf{h}_{i+\frac{1}{2}}^-)$ as an example. Let

$$\mathcal{P}(\mathbf{h}_{i+\frac{1}{2}}^-) = Q^T \Pi Q,$$

489 be the eigenvalue decomposition for $\mathcal{P}(\mathbf{h}_{i+\frac{1}{2}}^-)$, where $\Pi = \text{diag}(\lambda_1, \dots, \lambda_K)$. For
 490 $k = 1, \dots, K$ and a given $\epsilon > 0$, define

491 (4.22)
$$\Pi^{\text{cor}} = \text{diag}(\lambda_1^{\text{cor}}, \dots, \lambda_K^{\text{cor}}), \quad \lambda_k^{\text{cor}} = \frac{\sqrt{2}\lambda_k}{\sqrt{\lambda_k^4 + \max\{\lambda_k^4, \epsilon^4\}}}.$$

493 In our scheme we choose $\epsilon = \Delta x$. Then, the corrected PCE coefficient vector for the
 494 velocity $\mathbf{u}_{i+\frac{1}{2}}^-$ is given by

495 (4.23)
$$\mathbf{u}_{i+\frac{1}{2}}^- = Q^T \Pi^{\text{cor}} Q \mathbf{q}_{i+\frac{1}{2}}^-.$$

496 For well-conditioned $\mathcal{P}(\mathbf{h}_{i+\frac{1}{2}}^-)$, the correction (4.23) reduces to the system (2.18), but
 497 when $\mathcal{P}(\mathbf{h}_{i+\frac{1}{2}}^-)$ is near singular, the discharge needs to be recomputed,

498 (4.24)
$$\mathbf{q}_{i+\frac{1}{2}}^- = \mathcal{P}(\mathbf{h}_{i+\frac{1}{2}}^-) \mathbf{u}_{i+\frac{1}{2}}^-,$$

499 in order to keep the scheme consistent.

500 *Remark 4.5.* If there is no uncertainty, the correction (4.22)-(4.23) reduces to the
 501 deterministic velocity desingularization in [23, 19].

502 **5. Numerical Results.** In this section, we summarize numerical tests to illustrate
 503 robustness of the proposed schemes for the SGSWE system (2.16) with different
 504 uncertainty models and parametric distributions. For simplicity we consider only
 505 one-dimensional stochastic spaces ($d = 1$) associated to a Beta density over $[-1, 1]$,

506
$$\rho(\xi) := \rho^{(\alpha, \beta)}(\xi) = C(\alpha, \beta)(1 - \xi)^\alpha(1 + \xi)^\beta, \quad C(\alpha, \beta)^{-1} = 2^{\alpha+\beta+1} B(\beta + 1, \alpha + 1)$$

508 where $B(\cdot, \cdot)$ is the Beta function, and the parameters $\alpha, \beta > -1$ can be chosen freely
 509 and control how mass concentrates at $\xi = 1$ and $\xi = -1$, respectively. In particular
 510 $\alpha = \beta = 0$ corresponds to the uniform distribution on $[-1, 1]$. The numerical examples
 511 in the coming sections consist of the following numerical experiments:

512 • **subsection 5.1:** Stochastic bottom topography model, comparing the SGSWE so-
 513 lution (2.16) with $K = 9$ and $K = 17$ with the uniform density, $\alpha = \beta = 0$. The
 514 results are compared against a $K = 9$ stochastic collocation solution computed with

515 $S = 100$ stochastic points. The stochastic collocation solution for, e.g., the water
 516 height h , is computed via quadrature,

$$517 \quad h_{SC}(x, t, \xi) := \sum_{j=1}^K \hat{h}_{SC,j}(x, t) \phi_k(\xi), \quad \hat{h}_{SC,j}(x, t) := \sum_{s=1}^S h(x, t, \zeta_s) \phi_j(\zeta_s) z_s$$

519 where $\{\zeta_s, z_s\}_{s=1}^S$ is the S -point ρ -Gaussian quadrature rule, and $h(x, t, \zeta_s)$ is a
 520 numerical solution to a deterministic specialization of the SWE (2.2) obtained by
 521 setting $\xi = \zeta_s$ and numerically solved using a deterministic central-upwind scheme.

- 522 • **subsection 5.2:** Stochastic water surface model, testing the well-balanced property
 523 of the scheme with $\alpha = \beta = 0$
- 524 • **subsection 5.3:** Stochastic discontinuous bottom topography model, investigating
 525 the effects of different values of M used to enforce $\mathcal{P}(\hat{h}) > 0$. This example also
 526 investigates different distributions, with $(\alpha, \beta) = (3, 1)$ and $(\alpha, \beta) = (1, 3)$.

527 The parameter θ in the generalized minmod limiter is set to $\theta = 1.3$ for the first
 528 two examples, and $\theta = 1$ for the third example. The gravitational constant g is set
 529 to $g = 1$ for the first two examples, and $g = 2$ for the last example. We filter only
 530 the water heights h_Λ except in the very last numerical test. In the third numerical
 531 example, when $(\alpha, \beta) = (1, 3)$, we filter both the water heights and the discharges
 532 of the water. In all examples, the CFL condition we use in our simulation is (4.16).
 533 However, we observe that in practice, a relaxed time step $c\Delta t^n (c > 1)$ will not result
 534 in loss of hyperbolicity and the plots are similar visually to the results obtained from
 535 the condition (4.16). We believe this is because condition (3.7) is only a sufficient but
 536 not a necessary condition to the hyperbolicity of SGSWE.

537 Our numerical results will report quantile regions indicating the range of behavior
 538 for solutions. These quantile regions are computed empirically by computing the
 539 corresponding PCEs on 10^5 randomly sampled points from the density ρ on $[-1, 1]$.

540 For a fixed spatial grid, the computational cost depends on the dimension K of the
 541 chosen polynomial subspace P_Λ . In order to compute the propagation speeds (4.1),
 542 the eigenvalues of the $2K \times 2K$ Jacobian $J(\mathbf{U})$ matrix must be computed, making
 543 this cost increase as K increases. In addition, to preserve hyperbolicity, we need to
 544 ensure the positivity of the water height at all the quadrature points for every spatial-
 545 temporal point (Theorem 3.1). Therefore, the cost for preserving the hyperbolicity
 546 is at most of order $O(K^3)$ per cell per time step (Corollary 3.5). These relations are
 547 formally independent of the dimension d of the stochastic space, but in practice K
 548 can grow considerably as d is increased. For example, one may choose P_Λ to be the
 549 space of the polynomials with degree up to L . In this case, $K = \binom{L+d}{d}$. When $L \geq d$,
 550 as d increases, K increases and also therefore does the computational cost. In this
 551 paper, we only consider numerically the case $d = 1$. We plan to investigate higher
 552 dimensional stochastic space in a future work. However, note that the developed
 553 theory in section 2 and section 3 extends to $d > 1$.

554 **5.1. Stochastic Bottom Topography.** We consider the shallow water system
 555 with deterministic initial conditions

$$556 \quad (5.1) \quad w(x, 0) = \begin{cases} 1 & x < 0 \\ 0.5 & x > 0 \end{cases}, \quad q(x, 0) = 0,$$

557 and with a stochastic bottom topography

$$558 \quad (5.2) \quad B(x, \xi) = \begin{cases} 0.125(\cos(5\pi x) + 2) + 0.125\xi, & |x| < 0.2 \\ 0.125 + 0.125\xi, & \text{otherwise} \end{cases}.$$

559 In this example, we model ξ as a uniform random variable ($\alpha = \beta = 0$). The cor-
 560 responding orthonormal basis functions ϕ_j are the orthonormal Legendre polynomials
 561 on $[-1, 1]$ with density $\rho(\xi) = \frac{1}{2}$. Initially, the highest possible bottom barely touches
 562 the initial water surface at $x = 0.5$. In [Figure 1](#) and [Figure 2](#), we use a uniform
 563 grid size Δx over the physical domain $x \in [-1, 1]$, and compute up to terminal time
 564 $t = 0.8$. We present the numerical solutions for $K = 9$ and $K = 17$ using $M = 17$
 565 and $M = 33$ -point Gaussian quadrature nodes, respectively, to enforce the positivity
 condition [\(3.7\)](#).

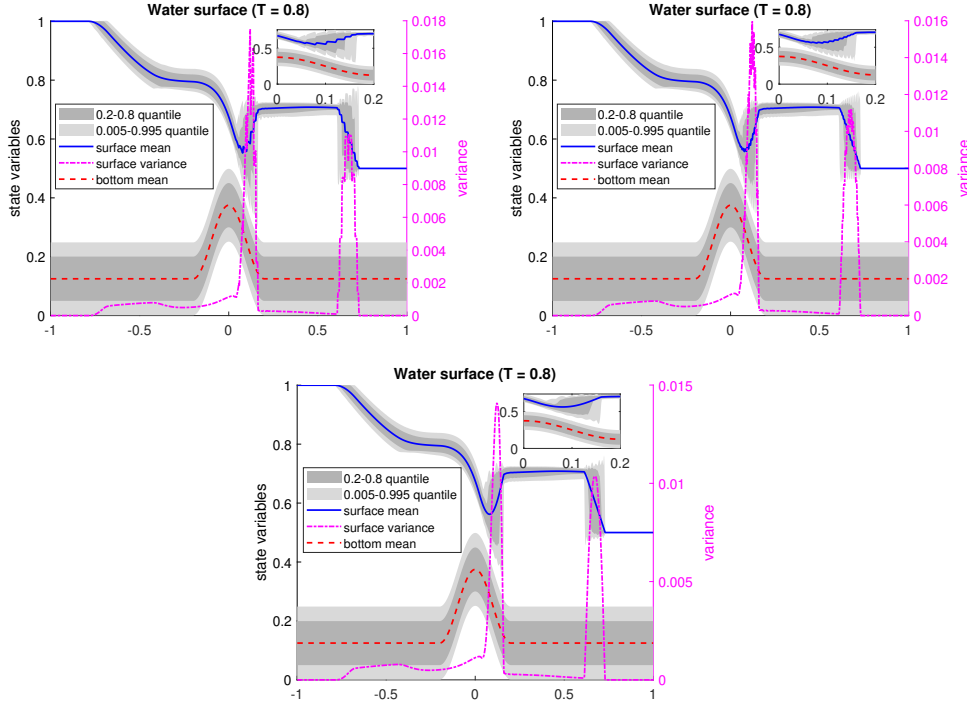


FIG. 1. Results for [subsection 5.1](#), water surfaces. Top left: stochastic Galerkin, $K = 9$, $\Delta x = 1/800$. Top right: stochastic Galerkin, $K = 17$, $\Delta x = 1/800$. Bottom: stochastic collocation, $K = 9$, $\Delta x = 1/800$.

566 The 99% confidence region of the water surface stays above the 99% confidence
 567 region of the bottom function in the first three (top left, top right, bottom left)
 568 subfigures in [Figure 1](#).

569 For reference and comparison, a solution obtained by the stochastic collocation
 570 method (100 quadrature points, $K = 9$ -term PCE as explained in [section 5](#)) is com-
 571 puted. Results for water surface and discharge are shown in the right subfigures of
 572 [Figure 1](#) and [Figure 2](#), respectively. We note that the stochastic collocation solution is
 573 a different PDE model, so we do not necessarily expect the numerical results from the
 574 SG and SC solvers to be identical for a fixed, finite K . In particular, we do not expect
 575 “convergence” of one model to the other as, say $S \uparrow \infty$ and/or $\Delta x \downarrow 0$. However,
 576 the results in the figures do show substantial similarity between these solutions. The
 577 numerical solution obtained from the collocation method is less oscillatory near sharp
 578 gradients of water surface and discharges.

579 We observe small oscillations near sharp gradients of the water surface and dis-

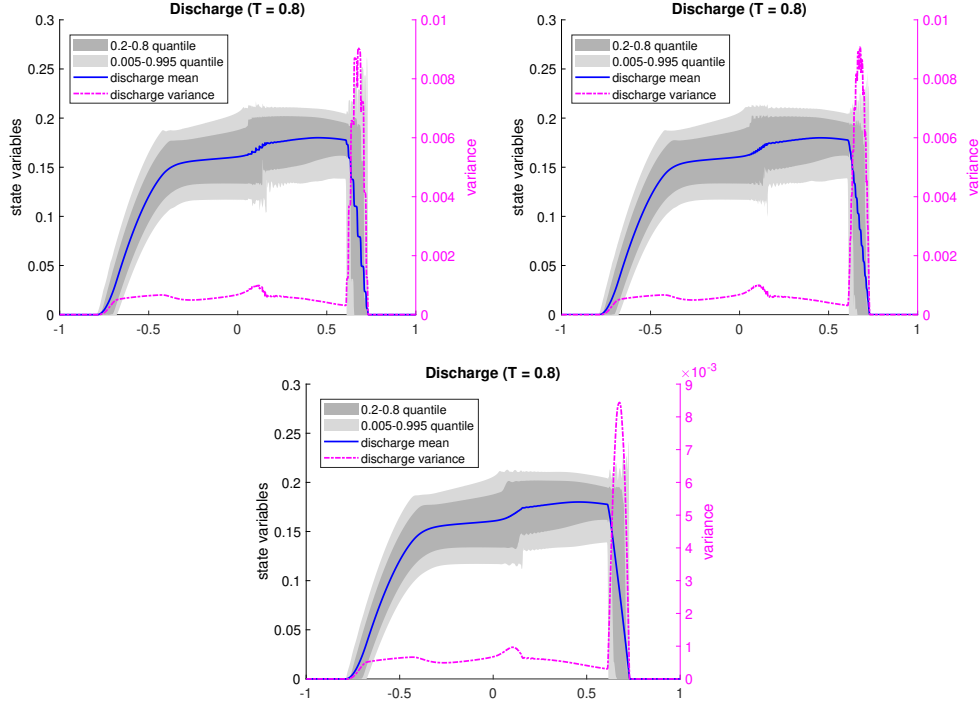


FIG. 2. Results for subsection 5.1, discharges. Top left: stochastic Galerkin, $K = 9, \Delta x = 1/800$. Top right: stochastic Galerkin, $K = 17, \Delta x = 1/800$. Bottom: stochastic collocation, $K = 9, \Delta x = 1/800$.

charge in all of the figures. We investigate the oscillations for the discharge more carefully in Figure 3. We observe that both higher resolution and larger K can reduce the magnitude of the oscillations that appear in quantiles.

5.2. Stochastic Water Surface. Consider a stochastic shallow water system with a deterministic bottom function

$$586 \quad (5.3) \quad B(x, \xi) = \begin{cases} 10(x - 0.3), & 0.3 \leq x \leq 0.4, \\ 1 - 0.0025 \sin^2(25(\pi(x - 0.4))), & 0.4 \leq x \leq 0.6, \\ -10(x - 0.7), & 0.6 \leq x \leq 0.7, \\ 0 & \text{otherwise,} \end{cases}$$

587 and a stochastic water surface,

$$588 \quad (5.4) \quad w(x, 0, \xi) = \begin{cases} 1.001 + 0.001\xi & 0.1 < x < 0.2, \\ 1 & \text{otherwise,} \end{cases} \quad q(x, 0, \xi) \equiv 0.$$

589 We again model ξ as a uniform random variable ($\alpha = \beta = 0$) with $K = 9$. A small
590 uncertain region was originally at $0.1 \leq x \leq 0.2$, where the water surface is slightly
591 perturbed. The 17-point ρ -Gaussian quadrature rule is used to enforce the condition
592 (3.7) to guarantee hyperbolicity. We compute the cell averages of the vector of PCE
593 coefficients for water surface and discharges at terminal time $t = 1.0$ on the physical
594 domain $[-1, 1]$ with uniform grid size $\Delta x = 1/400$. We observe from the mid figure of

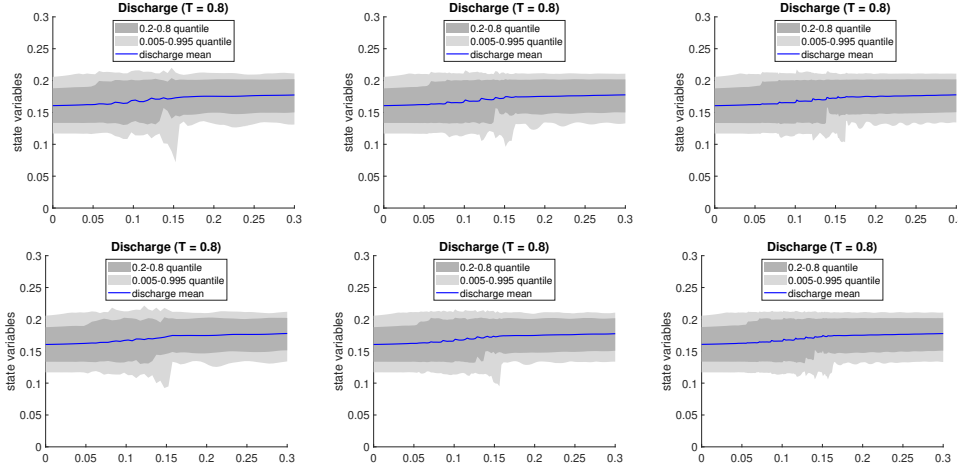


FIG. 3. Results for subsection 5.1, discharges on $[0, 0.3]$ for different values of K and Δx , zoom view. Top: $K = 9$; bottom: $K = 13$. Left: $\Delta x = 1/200$; middle: $\Delta x = 1/400$; right $\Delta x = 1/800$.

595 Figure 4 that the perturbed water surface with uncertainties propagate along different
 596 directions. The right-moving wave interacts with the nonflat bottom and get partially
 597 reflected. The magnitude of the uncertainties doesn't seem to exceed the magnitude
 598 of the initial uncertainties, which illustrate the well-balanced property of our scheme.

599 **5.3. Stochastic Discontinuous Bottom.** For our last example, consider the
 600 shallow water system with deterministic initial conditions,

$$601 \quad (5.5) \quad w(x, 0, \xi) = \begin{cases} 5.0 & x \leq 0.5, \\ 1.6 & x > 0.5, \end{cases} \quad u(x, 0, \xi) = \begin{cases} 1.0 & x \leq 0.5, \\ -2.0 & x > 0.5, \end{cases}$$

602 and a stochastic discontinuous bottom

$$603 \quad (5.6) \quad B(x, \xi) = \begin{cases} 1.5 + 0.1\xi & x \leq 0.5, \\ 1.1 + 0.1\xi & x > 0.5, \end{cases}$$

604 where initially we model ξ as a random variable with Beta density defined by $(\alpha, \beta) =$
 605 $(3, 1)$, which is more concentrated toward $\xi = -1$, and hence the bottom topography
 606 has higher probability of having smaller values. At time $t = 0$, the highest possible
 607 bottom barely touches the initial water height at $x = 0.5$. We compute the numerical
 608 solutions of $K = 9$ -term PCE with an $M = 17$ -point ρ -Gaussian quadrature to enforce
 609 the condition (3.7). We compute on a physical domain $x \in [0, 1]$ with uniform cell
 610 size $\Delta x = 1/400$ up to terminal time $t = 0.15$.

611 In this example we observe over- and undershoots in the neighborhood of the
 612 bottom discontinuity for both the water surface w and the discharge q (see Figure 5).
 613 This phenomenon also occurs in deterministic version of (5.5)-(5.6) when numerical
 614 solutions are computed using the schemes from [1, 32]. In addition we observe in this
 615 example a numerical artifact resulting from our enforcement of positivity of the water
 616 height (3.7) at only a finite number of points: although the 99% quantile region of
 617 water heights lies above 0, the ξ -global minimum of the water height in some cells
 618 can still be negative. Since $\mathcal{P}(\hat{h}) > 0$ only requires positivity of h_Λ at a finite number
 619 of points, there are (low-probability) regions of the domain where the height can be

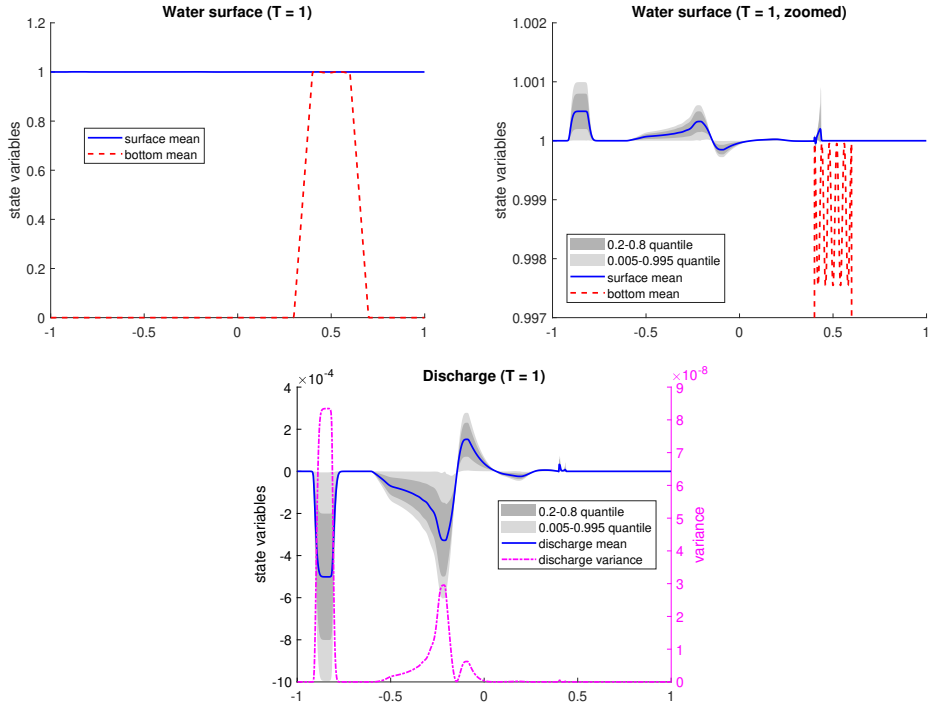


FIG. 4. Results for subsection 5.2: water surface (left), zoomed water surface (mid), and discharge (right) at $t = 1$ for (5.3)-(5.4), $K = 9$.

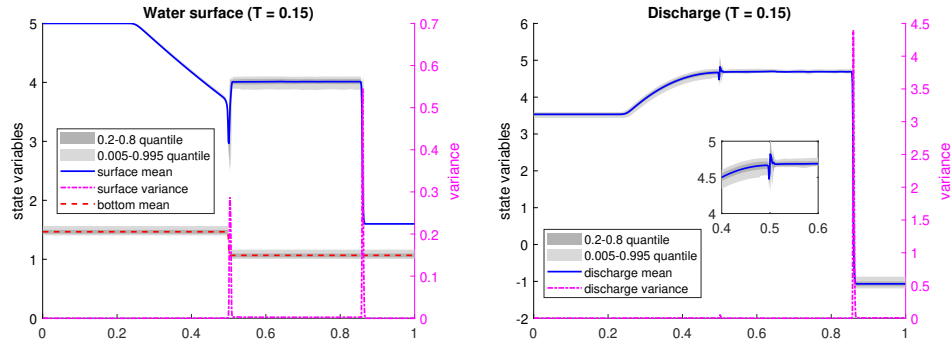


FIG. 5. subsection 5.3 results: $K = 9$, $t = 0.15$, $(\alpha, \beta) = (3, 1)$. Left figure: water surface and bottom. Right figure: discharge.

620 negative. Note, however, that the SGSWE system is still hyperbolic and simulation
621 can continue, despite low probability of negative water height.

622 Nevertheless, the existence of negative water heights impose doubts on the ap-
623 plicability of the SGSWE model. Fortunately, this situation can be mitigated by
624 increasing the number of points M where positivity of h_Λ is enforced. We observe
625 that if the positivity of the water height is enforced at more points, the stochastic
626 region of negative height shrinks. We demonstrate this with results in Table 1. In
627 particular we observe that (a) the negative region occurs on a subinterval containing

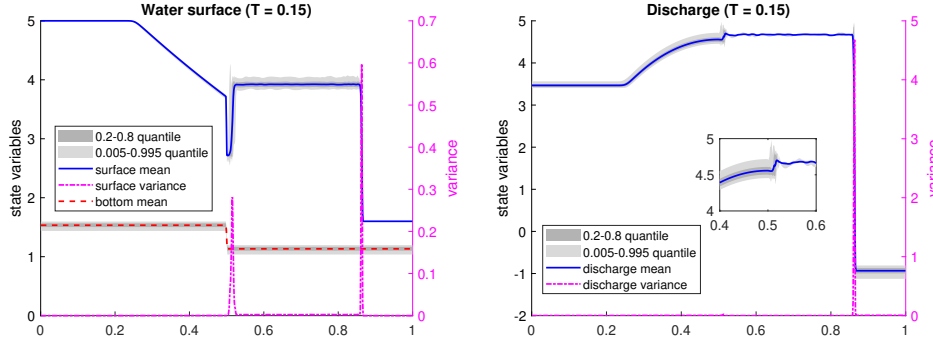
M	$\max_m \xi_m$	Negative Region N_M	$\Pr[\xi \in N_M]$
15	0.934077	[0.934079, 1]	5.75×10^{-6}
17	0.946839	[0.946899, 1]	2.43×10^{-6}
19	0.956205	[0.956320, 1]	1.12×10^{-6}
21	0.963310	[0.963398, 1]	5.18×10^{-7}

TABLE 1

Numerical study of ξ -region and associated probabilities where the water height is negative.

628 ξ values greater than the maximum quadrature point, and (b) the probability of ξ
 629 lying in this region is quite small.

630 In a separate experiment, we also compute the numerical results when ξ is modeled
 631 as random according to a $(\alpha, \beta) = (1, 3)$ distribution, which is more concentrated
 632 toward $\xi = 1$. Figure 6 shows that at the terminal time the “pressure” from stochastic
 633 bottom that skews positively causes more oscillations on the water surface and the
 634 discharge compared to Figure 5. In this experiment, we filter both the water heights
 and the discharges.

FIG. 6. Numerical results with $(\alpha, \beta) = (1, 3)$, $K = 9$, $t = 0.15$. Left figure: water surface and bottom. Right figure: discharge.

635

636 **Appendix A. The Semi-Discrete Second-Order Central-Upwind**

637 **Scheme.** We briefly describe the central-upwind schemes for 1-D balance laws. For
 638 a complete description and derivation, we refer to [22]. Consider the balance law,

639 (A.1)
$$\mathbf{U}_t + (F(\mathbf{U}))_x = S(\mathbf{U})$$

640 For a uniform mesh with cells $\mathcal{C}_i := [x_{i-1/2}, x_{i+1/2}]$ of size $|\mathcal{C}_i| \equiv \Delta x$, centered at
 641 $x_i = (x_{i-1/2} + x_{i+1/2})/2$, and assume that at certain a time level, the cell averages

642 (A.2)
$$\bar{\mathbf{U}}_i^n \approx \frac{1}{\Delta x} \int \mathbf{U}_i(t^n) dx := \frac{1}{\Delta x} \int_{\mathcal{C}_i} \mathbf{U}(x, t^n) dx$$

643 are available. The cell averages are then used to construct a non-oscillatory second-
 644 order linear piecewise reconstructions,

645 (A.3)
$$\tilde{\mathbf{U}}_i^n(x) = \bar{\mathbf{U}}_i^n + (\mathbf{U}_x)_i(x - x_i), \quad x \in \mathcal{C}_i,$$

646 whose slopes $(\mathbf{U}_x)_i$ are obtained by generalized minmod limiter,

647 (A.4)
$$(\mathbf{U}_x)_i = \text{minmod} \left(\theta \frac{\mathbf{U}_{i+1}^n - \mathbf{U}_i^n}{\Delta x}, \frac{\mathbf{U}_{i+1}^n - \mathbf{U}_{i-1}^n}{2\Delta x}, \theta \frac{\mathbf{U}_i^n - \mathbf{U}_{i-1}^n}{\Delta x} \right),$$

648 where the minmod function is defined to be

$$649 \quad \text{minmod}(z_1, z_2, \dots) := \begin{cases} \min\{z_1, z_2, \dots\} & \text{if } z_i > 0, \forall i, \\ \max\{z_1, z_2, \dots\} & \text{if } z_i < 0, \forall i, \\ 0 & \text{otherwise,} \end{cases}$$

650 and the parameter $\theta \in [1, 2]$ controls the amount of numerical dissipation. The left-
651 and right-sided reconstructions at the endpoints of \mathcal{C}_i are,

$$652 \quad (\text{A.5}) \quad \mathbf{U}_{i-\frac{1}{2}}^+ = \bar{\mathbf{U}}_i^n - \frac{\Delta x}{2}(\mathbf{U}_x)_i, \quad \mathbf{U}_{i+\frac{1}{2}}^- = \bar{\mathbf{U}}_i^n + \frac{\Delta x}{2}(\mathbf{U}_x)_i.$$

653 The semidiscrete form of the central-upwind scheme is then given by,

$$654 \quad (\text{A.6}) \quad \frac{d}{dt} \bar{\mathbf{U}}_i(t) = -\frac{\mathcal{F}_{i+\frac{1}{2}} - \mathcal{F}_{i-\frac{1}{2}}}{\Delta x} + \bar{\mathbf{S}}_i,$$

655 where the numerical flux \mathcal{F} and the source term $\bar{\mathbf{S}}_i$ are given in (4.3) and (4.2),
656 respectively.

657 **Appendix B. Proof of Corollary 3.5.** The Corollary is immediate from the
658 following Lemma:

659 **LEMMA B.1.** *For some $M \leq \dim P_\Lambda^3$, there is an M -point positive quadrature rule
660 that is exact on P_Λ^3 .*

661 The veracity of this lemma immediately yields $M \leq \dim P_\Lambda^3$ in **Corollary 3.5**. The
662 second bound in that corollary results from chaining this with the dimension bound
663 in (2.3). Thus, we need only prove the above Lemma, which in turn is a simple
664 consequence of Tchakaloff's theorem:

665 **LEMMA B.2** (Tchakaloff's Theorem, [3]). *Let $P_{T,\ell}$ denote the space of polynomi-
666 als of degree up to ℓ on \mathbb{R}^d :*

$$667 \quad P_{T,\ell} := \text{span} \left\{ \zeta^\nu \mid \sum_{J=1}^d \nu_J \leq \ell \right\}.$$

668 *Then for some $M \leq \dim P_{T,\ell}$, there exists a set of quadrature nodes $\{\zeta_m\}_{m=1}^M$ and
669 positive weights $\{\tau_m\}_{m=1}^M$ such that*

$$671 \quad \int_{\mathbb{R}^d} p(\zeta) \rho(\zeta) d\zeta = \sum_{m=1}^M p(\zeta_m) \tau_m, \quad p \in P_{T,\ell}.$$

673 Now given P_Λ^3 , let ℓ^* denote the maximum polynomial degree of any element in P_Λ^3 :

$$674 \quad \ell^* := \sup_{p \in P_\Lambda^3} \deg p = \max_{k=1, \dots, K} \deg \phi_k,$$

676 which is finite. Then clearly we have $P_\Lambda^3 \subseteq P_{T,\ell^*}$. By **Lemma B.2**, there is some
677 $M^* \leq \dim P_{T,\ell^*}$ such that $\{\zeta_m^*\}_{m=1}^{M^*}$ and $\{\tau_m^*\}_{m=1}^{M^*}$ are nodes and (positive) weights,
678 respectively, corresponding to a quadrature rule that is exact on P_Λ (since it's exact on
679 the larger set P_{T,ℓ^*}). Note that if $M^* \leq \dim P_\Lambda^3 =: Q$, then the result of **Lemma B.1** is
680 immediate, so we assume otherwise. Let $\{\psi_k\}_{k=1}^Q$ denote any basis for P_Λ^3 , and define

$$682 \quad \Psi(\zeta) := [\psi_1(\zeta), \psi_2(\zeta), \dots, \psi_Q(\zeta)]^T \in \mathbb{R}^Q.$$

683 Then exactness of the quadrature rule on P_Λ^3 implies the vector-valued equality,

684
$$\sum_{m=1}^{M^*} \tau_m^* \Psi(\zeta_m^*) = \mathbf{e}, \quad (e)_k := \int_{\mathbb{R}^d} \psi_k(\zeta) \rho(\zeta) d\zeta.$$

 685

686 I.e., $\mathbf{e} \in \mathbb{R}^Q$ lies in the convex hull of $\{\Psi(\zeta_m^*)\}_{m=1}^{M^*}$. By Carathéodory's Theorem,
 687 there must be a size- Q subset of nodes $\{\zeta_m\}_{m=1}^Q \subset \{\zeta_m^*\}_{m=1}^{M^*}$, with positive weights
 688 $\{\tau_m\}_{m=1}^Q$, such that $\sum_{m=1}^Q \tau_m \Psi(\zeta_m) = \mathbf{e}$, which proves Lemma B.1.

689 REFERENCES

690 [1] E. AUDUSSE, F. BOUCHUT, M.-O. BRISTEAU, R. KLEIN, AND B. T. PERTHAME, *A fast and*
 691 *stable well-balanced scheme with hydrostatic reconstruction for shallow water flows*, SIAM
 692 *Journal on Scientific Computing*, 25 (2004), pp. 2050–2065.
 693 [2] I. BABUSKA, R. TEMPONE, AND G. E. ZOURARIS, *Galerkin finite element approximations of*
 694 *stochastic elliptic partial differential equations*, SIAM Journal on Numerical Analysis, 42
 695 (2004), pp. 800–825.
 696 [3] C. BAYER AND J. TEICHMANN, *The proof of Tchakaloff's Theorem*, Proceedings of the American
 697 Mathematical Society, 134 (2006), pp. 3035–3040.
 698 [4] S. BOYD, S. P. BOYD, AND L. VANDENBERGHE, *Convex optimization*, Cambridge university
 699 press, 2004.
 700 [5] S. BRYSON, Y. EPSHTEYN, A. KURGANOV, AND G. PETROVA, *Well-balanced positivity preserving*
 701 *central-upwind scheme on triangular grids for the Saint-Venant system*, ESAIM: Mathematical
 702 Modelling and Numerical Analysis, 45 (2011), pp. 423–446.
 703 [6] A. CHERTOCK, S. CUI, A. KURGANOV, AND T. WU, *Well-balanced positivity preserving central-*
 704 *upwind scheme for the shallow water system with friction terms*, International Journal for
 705 numerical methods in fluids, 78 (2015), pp. 355–383.
 706 [7] A. CHERTOCK, S. JIN, AND A. KURGANOV, *A well-balanced operator splitting based stochastic*
 707 *Galerkin method for the one-dimensional Saint-Venant system with uncertainty*, preprint,
 708 (2015).
 709 [8] A. CHERTOCK, S. JIN, AND A. KURGANOV, *An operator splitting based stochastic Galerkin*
 710 *method for the one-dimensional compressible Euler equations with uncertainty*, preprint,
 711 (2015), pp. 1–21.
 712 [9] A. J.-C. DE SAINT-VENANT, *Théorie du mouvement non-permanent des eaux, avec application*
 713 *aux crues des rivières et à l'introduction des marées dans leur lit*, CR Acad. Sci. Paris, 73
 714 (1871), p. 5.
 715 [10] B. J. DEBUSSCHERE, H. N. NAJM, P. P. PÉBAY, O. M. KNIO, R. G. GHANEM, AND O. P.
 716 *LE MAÎTRE*, *Numerical challenges in the use of polynomial chaos representations for sto-*
 717 *chastic processes*, SIAM journal on scientific computing, 26 (2004), pp. 698–719.
 718 [11] B. DESPRÉS, G. POËTTE, AND D. LUCOR, *Robust uncertainty propagation in systems of conser-*
 719 *vation laws with the entropy closure method*, in *Uncertainty quantification in computational*
 720 *fluid dynamics*, Springer, 2013, pp. 105–149.
 721 [12] M. EIGEL, C. J. GITTELSON, C. SCHWAB, AND E. ZANDER, *Adaptive stochastic Galerkin fem*,
 722 *Computer Methods in Applied Mechanics and Engineering*, 270 (2014), pp. 247–269.
 723 [13] O. G. ERNST, A. MUGLER, H.-J. STARKLOFF, AND E. ULLMANN, *On the Convergence of Gen-*
 724 *eralized Polynomial Chaos Expansions*, ESAIM: Mathematical Modelling and Numerical
 725 *Analysis*, 46 (2012), pp. 317–339.
 726 [14] S. GERSTER AND M. HERTY, *Entropies and symmetrization of hyperbolic stochastic Galerkin*
 727 *formulations*, Comm. Computat. Phys., to appear, (2020).
 728 [15] S. GERSTER, M. HERTY, AND A. SIKSTEL, *Hyperbolic stochastic Galerkin formulation for the*
 729 *p-system*, Journal of Computational Physics, (2019).
 730 [16] S. GOTTLIEB, C.-W. SHU, AND E. TADMOR, *Strong stability-preserving high-order time dis-*
 731 *cretization methods*, SIAM review, 43 (2001), pp. 89–112.
 732 [17] J. HU AND S. JIN, *A stochastic Galerkin method for the Boltzmann equation with uncertainty*,
 733 *Journal of Computational Physics*, 315 (2016), pp. 150–168.
 734 [18] S. JIN AND R. SHU, *A study of hyperbolicity of kinetic stochastic Galerkin system for the*
 735 *isentropic Euler equations with uncertainty*, Chinese Annals of Mathematics, Series B, 40
 736 (2019), pp. 765–780.

737 [19] A. KURGANOV, *Finite-volume schemes for shallow-water equations*, Acta Numerica, 27 (2018),
 738 pp. 289–351.

739 [20] A. KURGANOV AND D. LEVY, *Central-upwind schemes for the Saint-Venant system*, ESAIM: Mathematical Modelling and Numerical Analysis, 36 (2002), pp. 397–425.

740 [21] A. KURGANOV AND C.-T. LIN, *On the reduction of numerical dissipation in central-upwind
 741 schemes*, Commun. Comput. Phys., 2 (2007), pp. 141–163.

742 [22] A. KURGANOV, S. NOELLE, AND G. PETROVA, *Semidiscrete central-upwind schemes for hy-
 743 perbolic conservation laws and Hamilton-Jacobi equations*, SIAM Journal on Scientific
 744 Computing, 23 (2001), pp. 707–740.

745 [23] A. KURGANOV AND G. PETROVA, *A second-order well-balanced positivity preserving central-
 746 upwind scheme for the Saint-Venant system*, Communications in Mathematical Sciences, 5 (2007), pp. 133–160.

747 [24] A. KURGANOV, G. PETROVA, AND B. POPOV, *Adaptive semidiscrete central-upwind schemes
 748 for nonconvex hyperbolic conservation laws*, SIAM Journal on Scientific Computing, 29 (2007), pp. 2381–2401.

749 [25] A. KURGANOV AND E. TADMOR, *New high-resolution central schemes for nonlinear conservation
 750 laws and convection–diffusion equations*, Journal of Computational Physics, 160 (2000), pp. 241–282.

751 [26] J. KUSCH, R. G. MCCLAREN, AND M. FRANK, *Filtered stochastic Galerkin methods for hy-
 752 perbolic equations*, Journal of Computational Physics, 403 (2020), p. 109073.

753 [27] O. LE MAÎTRE AND O. M. KNIO, *Spectral methods for uncertainty quantification: with appli-
 754 cations to computational fluid dynamics*, Springer Science & Business Media, 2010.

755 [28] X. LIU, J. ALBRIGHT, Y. EPSHTEYN, AND A. KURGANOV, *Well-balanced positivity preserving
 756 central-upwind scheme with a novel wet/dry reconstruction on triangular grids for the
 757 Saint-Venant system*, Journal of Computational Physics, 374 (2018), pp. 213–236.

758 [29] S. MISHRA, C. SCHWAB, AND J. SUKYS, *Multilevel Monte Carlo finite volume methods for
 759 shallow water equations with uncertain topography in multi-dimensions*, SIAM Journal on
 760 Scientific Computing, 34 (2012), pp. B761–B784.

761 [30] H. NESSYAHU AND E. TADMOR, *Non-oscillatory central differencing for hyperbolic conservation
 762 laws*, Journal of computational physics, 87 (1990), pp. 408–463.

763 [31] F. NOBILE, R. TEMPONE, AND C. G. WEBSTER, *A sparse grid stochastic collocation method
 764 for partial differential equations with random input data*, SIAM Journal on Numerical
 765 Analysis, 46 (2008), pp. 2309–2345.

766 [32] B. PERTHAME AND C. SIMEONI, *A kinetic scheme for the Saint-Venant system with a source
 767 term*, Calcolo, 38 (2001), pp. 201–231.

768 [33] P. PETTERSSON, G. IACCARINO, AND J. NORDSTRÖM, *A stochastic Galerkin method for the
 769 Euler equations with Roe variable transformation*, Journal of Computational Physics, 257 (2014), pp. 481–500.

770 [34] G. POËTTE, *Contribution to the mathematical and numerical analysis of uncertain systems of
 771 conservation laws and of the linear and nonlinear Boltzmann equation*, PhD thesis, 2019.

772 [35] G. POËTTE, B. DESPRÉS, AND D. LUCOR, *Uncertainty quantification for systems of conservation
 773 laws*, Journal of Computational Physics, 228 (2009), pp. 2443–2467.

774 [36] L. SCHLACHTER AND F. SCHNEIDER, *A hyperbolicity-preserving stochastic Galerkin approxima-
 775 tion for uncertain hyperbolic systems of equations*, Journal of Computational Physics, 375 (2018), pp. 80–98.

776 [37] R. SHU, J. HU, AND S. JIN, *A stochastic Galerkin method for the Boltzmann equation with
 777 multi-dimensional random inputs using sparse wavelet bases*, Numerical Mathematics:
 778 Theory, Methods and Applications, 10 (2017), pp. 465–488.

779 [38] G. SZEGÖ, *Orthogonal Polynomials*, American Mathematical Soc., 4th ed., 1975.

780 [39] J. TRYOEN, O. LE MAÎTRE, M. NDJINGA, AND A. ERN, *Intrusive Galerkin methods with up-
 781 winding for uncertain nonlinear hyperbolic systems*, Journal of Computational Physics, 229 (2010), pp. 6485–6511.

782 [40] N. WIENER, *The homogeneous chaos*, American Journal of Mathematics, 60 (1938), pp. 897–
 783 936.

784 [41] K. WU, H. TANG, AND D. XIU, *A stochastic Galerkin method for first-order quasilinear hyper-
 785 bolic systems with uncertainty*, Journal of Computational Physics, 345 (2017), pp. 224–244.

786 [42] D. XIU AND J. S. HESTHAVEN, *High-order collocation methods for differential equations with
 787 random inputs*, SIAM Journal on Scientific Computing, 27 (2005), pp. 1118–1139.

788 [43] D. XIU AND G. E. KARNIADAKIS, *The Wiener–Askey polynomial chaos for stochastic differential
 789 equations*, SIAM journal on scientific computing, 24 (2002), pp. 619–644.

790 [44] D. XIU AND J. SHEN, *Efficient stochastic Galerkin methods for random diffusion equations*,
 791 Journal of Computational Physics, 228 (2009), pp. 266–281.